CELL DAMAGE AND TISSUE REPAIR IN THE CENTRAL NERVOUS SYSTEM

ELECTRON MICROSCOPY STUDY OF NEURONAL DEATH AND CELL REPLACEMENT

Benita Andersson

Stockholm 2005

From the Department of Clinical Neuroscience
Karolinska Institutet, Stockholm, Sweden

CELL DAMAGE AND TISSUE REPAIR IN THE CENTRAL NERVOUS SYSTEM

ELECTRON MICROSCOPY STUDY OF NEURONAL DEATH AND CELL REPLACEMENT

Benita Andersson

Stockholm 2005

ISBN 91-7140-272-1
Repro-Print, Stockholm, Sweden
Cover page photograph “Brain’s cell” by Bertil Vallien

There is nothing permanent, only changes.
At each moment a change is the truth.

ABSTRACT

The central nervous system is vulnerable to various insults and particularly to ischemia. To mimic ischemia, a photochemical or compression lesion was induced in the right sensory motor cortex of rat brains. We studied the time course of ultrastructural changes in cortical neurones after lesioning, and the occurrence of different types of neuronal death was examined with respect to a potential therapeutic window. The lesion's appearance was documented by magnetic resonance imaging (MRI). At 0.5, 1, 3, 6, 12, 24, 48 and 72 hours post-lesion, cortical neurones were examined by electron microscopy (EM). Following a photochemical lesion, the neuropil in the lesioned area appeared disorganised at 0.5 h, while necrotic and apoptotic cells were identified as separate bodies. Three hours later the tissue was disintegrated. On the contralateral side, ruptured membranes were found at 3 h, which is a sign of irreversible cell death. Following a compression lesion, apoptotic cell death was most frequent at 12 h in the lesioned area, and signs of secondary delayed cell death, e.g. an enlarged endoplasmatic reticulum, were found at 3 h.

Following a cortical photochemical lesion, neurogenesis was studied after beam-walking and fluoxetine pre-treatment. Dividing cells, confirmed by bromodeoxyuridine staining and EM, migrated to the border of the lesion, and their number was enhanced after fluoxetine treatment.

Embryonic stem cells and bone marrow stromal cells, labelled with the iron-oxide nanoparticle Endorem®, were implanted into rat brains following a cortical photochemical lesion or a spinal cord compression lesion. Iron-containing cells, confirmed by Prussian blue staining and EM, were injected either into the contralateral hemisphere or intravenously into the femoral vein. The fate of labelled cells was tracked *in vivo* using MRI, which at seven and 14 days post-injection showed labelled cells migrating to the injury site.

The time course of ultrastructural changes in spinal cord neurones following a compression lesion was studied. EM showed at 0.5-6 h apoptotic and at 12-72 h necrotic cell death in the vicinity of the lesion.

The studies demonstrate that the chosen models are useful when studying ultrastructural changes in injured cells. As the morphology drastically changed at 3 h, the cellular alterations at this time point might represent a breakpoint at which cells either progress towards cell death or recover. Fluoxetine enhances stem cell migration towards a lesion. Endorem®-labelled stem cells remain viable and migrate to a lesion site; thus, Endorem® can be used for MRI tracking of implanted stem cells in animals and humans.

Key words: ischemia, cell death, repair, stem cells, neurogenesis, EM, MRI

LIST OF PUBLICATIONS

This thesis is based on the following publications, which are referred to by their Roman numerals:

I. Andersson B, Wu X, Bjelke B, Syková E.
Temporal profile of ultrastructural changes in cortical neurones after a photochemical lesion.
Journal of Neuroscience Research. 77:901-912, 2004

II. Andersson B, Bjelke B, Syková E.
Temporal profile of ultrastructural changes in cortical neurones after a compression lesion.
Submitted.

III. Šimonová Z, Andersson B, Námestková K, Lai LJ, Bjelke B, Syková E.
Neural stem cell proliferation and migration toward a photochemical lesion enhanced by beam walking and fluoxetine pretreatment.
Submitted.

IV. Jendelová P, Herynek V, DeCross J, Glogarová K, Andersson B, Hájek M, Syková E.
Imaging the fate of implanted bone marrow stromal cells labelled with superparamagnetic nanoparticles.
Magnetic Resonance in Medicine. 50:767-776, 2003

V. Jendelová P, Herynek V, Urdzíková L, Glogarova K, Kroupová J, Andersson B, Bryja V, Burian M, Hájek M, Syková E.
Magnetic resonance tracking of transplanted bone marrow and embryonic stem cells labelled by iron-oxide nanoparticles in rat brain and spinal cord.
Journal of Neuroscience Research. 76:232-234; 2004

VI. Andersson B, Urdzíková L, Burian M, Syková E.
Temporal-spatial pattern of spinal cord balloon compression lesion evaluated by electron microscopy and magnetic resonance imaging.
Manuscript.

LIST OF ABBREVIATIONS

ADCw	apparent diffusion coefficient of water
ATP	adenosine tri-phosphate
BrdU	bromodeoxyuridine
BW	body weight
CNS	central nervous system
DNA	deoxyribonucleinacide
eGFP	enhanced green fluorescent protein
ECC	oedematous cell changes
EDN	electron dense neurones
EM	electron microscopy
ER	endoplasmatic reticulum
ESCs	embryonic stem cells
EWN	electron weak neurones
FOV	field of view
GFAP	glial fibrillary acidic protein
GFP	green fluorescent protein
i.p.	intra peritoneal
i.v.	intra venous
ICC	ischemic cell changes
IgG	immunoglobulin
IU	international unit
HCC	homogenising cell changes
LM	light microscopy
MCAO	middle cerebral artery occlusion
MION	monocrystalline iron-oxide nanoparticle
MR	magnetic resonance
MRI	magnetic resonance imaging
MSCs	bone marrow stromal cells
NeuN	neuronal nuclear antigen
NMDA	*n*-methyl-*D*-aspartate
NO	nitric oxygen
PBS	phosphate buffered saline
PD	proton density
RNA	riboxynucleoacide
SGZ	subgranular zone
SPIO	superparamagnetic iron-oxide
SVZ	subventricular zone
T	Tesla
T_2	relaxation time
TE	echo time
TEM	transmission electron microscope
TR	repetition time
TUNEL	terminal deoxynucleotidyl transferas nick end labelling

TABLE OF CONTENTS

INTRODUCTION

General background

Injury in the central nervous system (CNS) causes cell damage or cell death. Severe injuries include stroke and spinal cord injuries, which in our society are two leading causes of death or adult disability. Following the initial damage from stroke, all surviving patients recover to some limited extent. However, most patients remain weak on one side, or hemi paretic: more than one-fifth are dependent on others for assistance with the activities of daily living, and about 30% live in nursing homes (Carmichael 2003). Also, following spinal cord injury, more than 88% of those who survive are forced to live in institutional residences or with living assistance (Becker et al. 2003). The health care costs and the estimated lifetime expenses are substantial. Furthermore, spinal cord injury affects mostly young people during the most productive period of their lives, with the average age at injury being 32 years. Stroke as well as spinal cord injury is therefore a considerable problem in modern society.

The physiological background of stroke and spinal cord injury is ischemia. Either a reduction in blood flow (hypoxia) or the total elimination of blood (anoxia) to parts of the brain causes ischemic brain tissue or stroke. This primary insult induces several toxic processes, including excitotoxicity, metabolic toxicity and oxidative stress, which produce CNS degeneration. The acute insult of spinal cord injury is usually compression or distraction, which is followed by progressive ischemia and degeneration in the surrounding tissues. Ischemia produces cell death and disability but also leads to a process of recovery and repair.

The most important clinical manifestation of the two disorders is functional impairment. Previous clinical studies demonstrated that recovery generally begins early after the insult, with the fastest improvement occurring during the first or two weeks (Nhan et al. 2004) (Bernhardt et al. 2004). However, most patients receive their first treatment many hours after symptom onset. Furthermore, in clinical trials no drug has been proven effective as an acute treatment. It is therefore of great importance to find time windows in which therapeutic interventions are relevant.

Recovery mechanisms and tissue repair following ischemia are not yet satisfactorily understood (Carmichael 2003). Advancements in stem cell research offer new possibilities for studying these processes. For a long time it was

believed that the mammalian CNS was incapable of self-repair and regeneration after injury (Björklund and Lindvall 2000). However, the situation has changed in the last decade. Neuronal stem cells with the ability to produce new neurones and glial cells remain in adulthood in some parts of the brain (Temple 2001), and stem cells have been successfully transplanted into animal models of ischemia or injury (Björklund et al. 2003) (Isacson 2003) (Silani and Leigh 2003). This opens up new strategies for recovery and repair.

Cell death and tissue repair

Cell birth and death are joined together. Cell death is important in tissue development, cell homeostasis and injury response. These processes, which also include cell proliferation, are widespread in most mammalian tissues, and we know today that they are also present in the nervous system. During early development, excess neurones and glial cells are produced, some of which later die leaving the required number of cells in the tissue. Stem cells in some specific areas in the mature nervous system constantly divide and then either differentiate or die. Following tissue damage, extensive neuronal and glial cell death is present, and today there is evidence showing that lost cell populations are replaced by new cells differentiated from stem cells.

STEM CELLS

Until recently, interest in stem cells was limited within neurobiology to studies of neuronal development. From single embryonic stem cells (ESCs), the nervous system develops by a process of division, differentiation and migration along complex lineages. Some of the early cells, or precursors, in the developmental lineage are stem cells. Stem cells are self-renewing; they divide to form copies of themselves, and they are pluripotent; they have the capacity to differentiate in response to different signals down a variety of lineages. Other precursors are progenitor cells; they are committed to a particular lineage and divide into new cells along the lineage and differentiate into a specific cell type. It has been the prevailing view that neuronal differentiation was completed during early development (Johansson 2003) (Gage 2000). However, the concept of the birth of new neurones in adulthood in the mammalian CNS (adult neurogenesis) is accepted today (Frisen et al. 1998) (Gage 2002). In the adult mammalian brain, new neurones are generated in mainly two regions. In the subventricular zone

(SVZ) lining the lateral ventricles, and in the subgranular zone (SGZ) of the hippocampal dentate gyrus, groups of astrocyte-like cells have been identified as neuronal stem cells, which not only differentiate into glial cells but also into neurones (Alvarez-Buylla et al. 2002) (Pleasure et al. 2000).

If we understand cell birth lineages during normal development, we might also be able to manipulate and control neural precursor cells *in vitro*, thus allowing expansion and controlled differentiation of neuronal stem cells, both *in vitro* and *in vivo.* Useful methods have been developed for culturing different types of stem cells and transplanting them into animal models of injury (Björklund and Lindvall 2000) (Björklund et al. 2003) (Isacson 2003). It has been shown that neuronal stem cells persist throughout life in many mammals, including humans (Temple 2001), and that progenitor cells can differentiate into neural tissue in the adult brain (Gage 2002) (Taupin and Gage 2002) (van Praag et al. 2002). After brain ischemia in animals, hippocampal pyramidal neurones have been shown to be recruited from endogenous neural progenitors (Nakatomi et al. 2002). Also, ischemia-induced neurogenesis in animals is thought to contribute to functional improvement (Abo et al. 2001). Electrical stimulation of previously paretic hind limbs activates new brain regions, contributing to recovery. This could be explained by enhanced neurogenesis. Furthermore, it was shown that antidepressant treatments increase the number of precursor cells in the dentate gyrus in adult rats (Malberg et al. 2000) and that learning enhances adult neurogenesis in the hippocampus (van Praag et al. 1999).

CELL DEATH

To study cell death, cell death has to be recognised. However, there is no well-defined point at which a cell dies (Lipton 1999). The most satisfactory definition of cell death is the point at which the cell becomes unable to recover its normal morphology and function: the point of no return. Today, we do not know enough of the death process to identify the point at which the cell biochemically and metabolically loses its function (Lipton 1999) (Carmichael 2003). Therefore, the best definition of cell death is the morphological one, i.e. ultimately the elimination of the cell from the tissue either by cell disintegration or phagocytosis (Lipton 1999).

Cell death is conventionally classified into two forms of death, namely *necrosis* and *apoptosis* (Kerr et al. 1972). Necrosis is always an abnormal event and results

entirely from outside influences. It involves a failure of cell homeostasis following injury, which is of such extent that it overwhelms the normal cellular mechanisms in the cell (Fawcett et al. 2001). The simplest necrotic pathways are events such as mechanical damage, causing a disruption of the cell membranes, or anoxia leading to a failure of ion membrane pumps and cellular swelling. However, damage that does not kill the cell immediately but initiates specific intra- and extracellular mechanisms may also lead to necrotic cell death. This can be seen in the nervous system following ischemia. Three types of ischemic cell death are described at the ultrastructural level: swollen "pale" neurones with oedematous cell changes (ECC), condensed "dark" neurones with ischemic cell changes (ICC) and disrupted "ghost" neurones with homogenising cell changes (HCC) (Lipton 1999).

Apoptosis has relatively recently been accepted as a cell death process in the vertebrate nervous system, although apoptotic cell death in the development of the nervous tissue of invertebrates has been well established for a long time (Fawcett et al. 2001). Apoptosis is an active process that involves an inherent cellular program leading to cell death and therefore is also called programmed cell death. The process requires energy and protein synthesis. Apoptosis, as it is seen in developmental tissue, differs morphologically and biochemically from necrosis. The main criteria are chromatin condensation with nuclear pycnosis, DNA fragmentation, membrane "blebbing" and cytoplasm shrinkage (Studzinski 1999). However, in the adult nervous system apoptosis following damage may appear with features similar to the features of necrosis. Still, apoptotic cell death is considered to be present in nervous tissue following injury, and the morphological features are subdivided into three different types of apoptosis (Fawcett et al. 2001). The first type has the classical star-shaped appearance with dense pycnotic nuclei and membrane "blebbing". Finally, apoptotic bodies are detached from the cell body. The second type is characterised by the formation of autophagic vacuoles and sometimes the dilation of mitochondria and the endoplasmic reticulum (ER). Some pycnotic nuclei and membrane "blebbing" might be seen. In type three neither pycnotic nuclei nor membrane "blebbing" is present, but rather a marked disintegration of the mitochondria, Golgi complex and ER. This type of apoptosis is morphologically similar to necrosis.

In order to distinguish whether necrosis or apoptosis is present, different approaches are used. DNA fragmentation, which is a hallmark of apoptosis, is detected by biochemical techniques such as TUNEL staining on tissue sections or DNA laddering in agarose gels. Prevention of cell death by inhibiting protein

synthesis, thus blocking apoptosis, is also a method to identify apoptosis. Another most reliable method is to observe structural changes under the microscope and ultimately to define the point at which the changes are irreversible and cell morphology cannot be recovered. The criteria of irreversible neuronal death are defined at the ultrastructural level. The two main criteria are dense flocculent mitochondria and cell membrane ruptures (Auer et al. 1985a) (Auer et al. 1985b) (Kalimo et al. 1977).

The *penumbra* zone

The region surrounding tissue with immediate cell death in the ischemic brain is the *penumbra* area. The *penumbra* zone is defined by different criteria; most straightforwardly, the *penumbra* is referred to as the area around the core of infarction where neurones do not communicate but are viable. Defined in static terms the zone is a cellular interface between the ischemic cells at the core of the infarction, which are committed to die, and unaffected cells in areas with normal blood flow (Hakim 1998). Defined as a zone of incomplete cerebral ischemia, where neurones are functionally inactive but still viable, the area is explained in biochemical terms (De Keyser et al. 1999). The literal translation: ”half shadow” of the Latin word *penumbra* perhaps best describes the area.

Within the *penumbra* zone cells do not die immediately but rather after a delay of some days. The cell death is not due to a rapid primary necrosis but to a cascade of secondary changes induced by the ischemic event. This “delayed cell death” has been shown to be mostly apoptotic (Fawcett et al. 2001). However, secondary delayed cell death *per se* is defined as a separate type of cell death. Secondary delayed cell death occurs following a brief trauma, not directly within a short time, but after a substantial time delay (Kermer et al. 1999) of some hours up to several days. The ultrastructural criteria are increasing stacks of ER, small dense bodies and the formation of large vacuoles (Lipton 1999), which differ from the criteria of apoptotic cell death. However, the affected neurones within the *penumbra* zone could, due to the time delay preceding cell death, be targets for neuroprotection (Kermer et al. 1999).

Background of the present work

Although neuronal death has been studied in experimental models of cerebral ischemia, the time course of ultrastructural changes in ischemic neurones has not been extensively studied. As an ischemic lesion progresses not only over time but also over an area, it is of importance, when examining the time course of changes, to determine a precise location for evaluating the tissue. It is therefore essential to use lesion models that are well-defined in location and size. Instead of using only one experimental model, different phases in the progression of ischemia can be studied separately in different models, and the results of the models, taken together, might give a better understanding of the progression of ischemia. Since most cells within the *penumbra* zone are viable, they have the capacity to restore their normal function and are therefore targets for therapeutic intervention. However, the cells are viable only for a limited period, and the time course of cell death in the *penumbra* zone is not yet known. Also, we know that new brain regions are activated after lesioning, and therefore ultrastructural changes, not only in the lesioned area but also on the corresponding contralateral side, are of interest for study. The time course of ultrastructural changes, correlated with behavioural tests and an *in vivo* evaluation of the lesion, gives the possibility to define time windows in which therapeutic interventions could be possible.

Processes of regeneration and tissue repair are activated by the ischemia itself, and we sought to study the contribution of endogenous and implanted stem cells to these processes. As cell death is complete in experimental models mimicking infarction, the best possibility to study tissue repair following ischemia might be to study it in such experimental models. We aimed to study whether the contribution of stem cells was enhanced after training, and therefore a unilateral lesion, induced in the locus for hind limb and forelimb functions, was useful. Different techniques to detect stem cells, endogenous as well as implanted, were used. In addition to conventional histology for optical microscopy to study the contribution of histochemically stained stem cells in the tissue, a new technique for labelling cells with superparamagnetic nanoparticles was developed (Wang et al. 2001) (Frank et al. 2003) (Bulte et al. 1999b). Nanoparticle-labelled cells can be visualised in the brain or spinal cord *in vivo* using MRI, and in tissue, at the ultrastructural level, using EM. By labelling stem cells with nanoparticles and by using histological techniques together with MRI and EM, we have the better possibility of tracking the fate of labelled cells.

MODELS OF ISCHEMIA

Different lesion models designed to mimic ischemia in animal brains or spinal cords have been established. We aimed to study ischemia of varying severity. To avoid a mixed pattern of morphological features when studying the time course of these features in ischemic brains, two models, well-defined in location and size, were used: a model of permanent cerebral ischemia mimicking the infarction and a model of temporary ischemia mimicking the *penumbra* zone. Rats were used in the experiments, and since the study included the evaluation of motor performance, ischemia was induced in the area of the sensory motor cortex in the rat brains. A spinal cord lesion model, which resembles a clinical spinal cord injury followed by ischemia, was chosen to study the contribution of stem cells to tissue repair in the spinal cord.

By using a photochemical lesion (Watson et al. 1985), a permanent cerebral ischemia can be induced in the brain. The photosensitive dye Rose Bengal, injected into rats, produces free radicals in the brain tissue when struck by white light. This photochemical reaction induces thrombosis, which leads to necrosis. The insult results in a lesion with sharp borders with healthy tissue; that is, the lesion lacks a *penumbra* zone.

A compression lesion in the brain produces temporary cerebral ischemia (Kundrotiené et al. 2002). Slow compression of the cortex causes a reduction in blood flow, thus resulting in moderate ischemia manifested as functional impairment. Since changes in the duration of the compression correlate well with the severity of ischemia, the model is well controlled and suitable for studying a *penumbra* zone where only a moderate reduction of blood flow is needed.

It is believed that in most experimental models of spinal cord injury, the primary pathogenesis is caused by the mechanical insult without the involvement of vascular factors. Thus, ischemic tissue due to primary insult is not present. However, the balloon-compression technique has proven to be a feasible method to produce a well-controlled spinal cord lesion in rats (Vanicky et al. 2001) followed by ischemia, mimicking well the clinical situation.

BEAM-WALKING TRAINING AND TESTING

Since functional outcome rather than infarction size determines the quality of life of stroke survivors, behavioural tests are as important as tissue analysis when studying ischemia, and different tests are used. As the natural tendency of a rat is to traverse a beam, a beam-walking test for motor performance is simple and natural. Standardised test protocols for a rat traversing a narrow elevated beam have been developed (Feeney et al. 1981), and the beam-walking test has been used to monitor motor function after a unilateral lesion in the sensory motor cortex (Boyeson et al. 1991).

The beam-walking test can be used as a model either for testing motor performance after lesioning or as a model for training and learning. To test motor function following a lesion, the animals are trained two days before the insult and thereafter tested each day. When studying the effects of training, the training period before the insult is usually longer and after lesioning the animals are tested each day.

IN VIVO EVALUATION OF THE LESION

MRI offers possibilities for the evaluation of ischemic tissue. The MRI method is based on imaging the proton or hydrogen nucleus. In biological tissue, the proton exists as hydrogen in free water molecules and water is present in different concentrations, therefore different tissues show varying signal intensities on magnetic resonance (MR) images. MRI is also sensitive to alterations in tissue water content. Not only the free movement of water molecules, e.g. Brownian motion, but also the water flow across the cell membrane during cell activity affects MR images.

Ischemia leads to alterations in tissue water content, and ischemic tissue can therefore be detected by MRI (Moseley et al. 1990). The degree of abnormal water movement can be determined from maps of the apparent diffusion coefficient of water (ADC_W) (Provenzale and Sorensen 1999) thus providing information about tissue water homeostasis. The T_2 relaxation time is measured as the relaxation time of protons that are out of phase in their internal magnetic fields. T_2 maps give information about proton motion and are affected by the inhomogeneities in the local magnetic field within the tissue. Damaged tissue, where hindering protein structures are disrupted, provides greater freedom for proton motion and

thus increased T_2 values (van Bruggen et al. 1992) (van der Toorn et al. 1996). Consequently, changes in T_2 values will indicate changes in the protein structure of a tissue. Proton density (PD) maps show the total number of protons in the tissue, i.e. the water content. The PD values are increased with greater water content, either due to leaking capillaries or a disrupted blood brain barrier, or because of changes in protein structure followed by water liberation.

SUPERPARAMAGNETIC NANOPARTICLES AS CONTRAST AGENTS

It has been shown that MRI can be used for the dynamic tracking of transplanted stem cells in animals (Yeh et al. 1995). Labelling the cells with contrast agents and then using MRI provides a non-invasive method for studying the fate of transplanted cells *in vivo* (Bulte et al. 1999a) (Bulte et al. 2001). Superparamagnetic iron-oxide nanoparticles can be used as contrast agents, and before transplantation, stem cells are labelled with the nanoparticles during incubation in cell culture.

In superparamagnetic nanoparticles, crystals of iron (Fe_2O_3FeO) are used as magnetic cores and a macromolecular shell formed of dextran, starch, polyol derivates or other polymers covers the crystals. (Wang et al. 2001) (Weissleder et al. 1997) (Yeh et al. 1993) (Yeh et al. 1993). The size of different types of nanoparticles can vary over a range of 4–150 nm (Brock 1989) (Bonnemain 1996). Specific antibodies can be attached to the shell, and thus the nanoparticles can bind specifically to cells (Bulte and Bryant 2001). The use of superparamagnetic nanoparticles as contrast agents in MRI leads to a shortening of T_2 relaxation times compared to those seen with standard paramagnetic contrast agents. Thus, it is possible to observe contrast changes on a cellular level.

ELECTRON MICROSCOPY

EM has been used as a standard tool in basic research since the first commercial electron microscopes were made available. Electron microscopes were developed due to the limitations of light microscopes and the desire to study fine details. The physics of light limits a light microscope to magnifications of 500x–1000x and a resolution of 0.2 μm. For studying details of cell ultrastructure, 100,000 x magnifications are needed. The transmission electron microscope (TEM) was the first type of electron microscope developed. The basic principles are the same as for

light microscopes except that a focused beam of electrons is used instead of light. A stream of electrons is formed by an electron gun, i.e. cathode, and accelerated in a vacuum column towards the specimen by using a positive electrical potential. Electromagnetic lenses focus the stream into a thin monochromatic beam, which strikes the specimen. Some of the electrons in the beam attach to heavy metals located in the cell membranes in the specimen and others are transmitted. The transmitted portion of the electrons is focused by objective lenses into an image on a phosphorous screen. In the images, details of nanometre size can be observed, since the optimal point resolution in TEM is 3 nm. The electron microscope is therefore a useful tool, not only when examining cell structure, but also when studying nanoparticle-labelled cells.

AIMS

In this thesis I focused on the following aims:

- To test which lesion models are useful when studying ischemic neurones at the ultrastructural level.

- To study the time course of ultrastructural changes in neurones following ischemia.

- To identify therapeutic time windows by correlating neuronal ultrastructure with functional recovery and lesion size.

- To study the contribution of endogenous and implanted adult and embryonic stem cells to lesion repair.

- To follow the differentiation of endogenous and implanted stem cells into neurones and glial cells by using cell specific markers.

- To follow the fate of implanted stem cells *in vivo* using superparamagnetic nanoparticle-labelled cells and magnetic resonance imaging.

- To use electron microscopy to follow the fate and differentiation of endogenous and implanted stem cells *in vitro*.

MATERIALS AND METHODS

Experimental animals (papers I-VI)

Male Sprague-Dawley and Wistar rats, six to eight weeks old, were used in the experiments. The rats were housed under standardised conditions regarding day/night cycle, temperature and humidity, with free access to water and food. Anaesthesia was induced by a mixture of 2-3% isoflurane/air and maintained during surgical procedures and MRI recordings at 1.5%. During surgery the body temperature was kept at 37- 38° C and constant cardiac and respiratory frequency was maintained.

The experiments were carried out in accordance with the European Communities Council Directive of 24th November 1986 (86/609/EEC). The experiments in papers I-III were approved by the local ethical committee, Stockholms norra djurförsöksetiska nämnd, Södra Roslags Tingsrätt, Stockholm, Sweden; project number N3/00 and the experiments in papers IV–VI by the local ethical committee of Institute of Experimental Medicine, Academy of Sciences, Prague, Czech Republic; project number: UEM 2003/2.

Lesion models (papers I-VI)

CORTICAL PHOTOCHEMICAL LESION

A photochemical lesion (papers I, III, IV, V) was induced in the right sensory motor cortex; the centre of the lesion was set to bregma –1.0 mm, 2.0 mm lateral to the midline according to the brain atlas of Paxinos and Watson (Paxinos and Watson 1986). Ten or 80 mg/kg BW of the photosensitive dye Rose Bengal was injected i.v. (60 μl/min) into the femoral vein. The dye was equilibrated in the blood pool for 90 s. The area of the lesion was exposed to the light from a halogen lamp for 10 or 15 min, while the rest of the skull was shielded with aluminium foil. A circular light beam, 8 mm in diameter, was focused at the lesion centre, and a homogeneous exposure was obtained by a slow 360° rotation of the beam during exposure. During illumination Rose Bengal is excited and generates molecular oxygen. Thus, the dye has the ability to induce a photoperoxidative reaction leading to thrombosis and infarction.

CORTICAL COMPRESSION LESION

To induce a compression lesion (paper II), a rat's head was fixed in a stereotaxic frame with the tooth bar at –3.3 to +1.5 mm. The maseter muscle was detached from the skull bone, and the centre of the lesion was outlined on the skull to bregma –1.0 mm, 3.5 mm lateral to the midline according to the brain atlas of Paxinos and Watson (Paxinos and Watson 1986). The skull bone over the lesion centre was removed from the dura mater and placed into sterile saline. Subsequently, a compressor piston was gently placed at the brain surface. The piston, made of Teflon, had a diameter of 8 mm with the medial part shortened by 2 mm, resulting in a medial-lateral distance of 6 mm. The edges of the piston were smoothed in order to avoid tissue damage of the brain surface. Angled 20° from the horizontal plane the piston was slowly lowered 2.8 mm towards the centre of the brain, and the compression was maintained for 30 min.

SPINAL CORD COMPRESSION LESION

A compression lesion was induced in the spinal cord by balloon inflation (papers V, VI). A 2 cm midline incision was cut over the L1-T10 spinous processes. Soft tissue and spinous processes of vertebrae T10-T11 were removed and the thoracic spinal column was fixed using haemostatic forceps held in a sterotactic frame, A hole with a diameter of 1.5 mm was drilled in vertebral arch of T10, using a dental drill. A 2-French Fogarty catheter was inserted into the dorsal epidural space through the hole and a spinal cord lesion was made at the T8-T9 spinal level by balloon inflation with a volume of 15 µl of saline for 5 min. Thereafter the catheter was deflated and removed. Inflation for 5 min produced paraplegia and was followed by gradual recovery.

Beam-walking test (papers I, III)

To measure motor function after lesioning, rats were subjected to beam-walking, including training and testing. For two days the rats were trained to traverse a narrow elevated beam. Starting at 24 h after lesioning, the rats were tested every day in traversing the beam. The test distance was 122 cm. Two persons independently rated motor function in a test with a 7 point rating scale. The rating was based on the number of foot slips of the hind limp (Table 1.). The test session started when the rat stayed balanced on the beam without assistance. The session ended when the contralateral hind limb passed the end point of the

beam, when 90 s were elapsed or when the rat fell off the beam. Training and testing sessions were conducted during the morning hours in a quiet room with dim lightning.

Table 1. Rating scale of motor function

7. Traverse the beam with no more than two foot slips.
6. Traverse the beam using the hind limb for more than 50% of the distance.
5. Traverse the beam using the hind limb for less than 50% of the distance.
4. Put the affected limb on the beam but cannot push off without slipping.
3. Traverse the test distance without using the affected limb.
2. Stay balanced on the beam but cannot traverse the test distance within 90s.
1. Fall off the beam.

Stem cell transplantation (papers IV, V)

Marrow stromal cells (MSCs) and ESCs were labelled with superparamagnetic iron-oxide nanoparticles and visualised, as described below, using phantoms and MRI, Thereafter stem cells were grafted into rats that were subjected to either a cortical or a spinal cord lesion.

CELL CULTURE

For the isolation of rat MSCs (papers IV, V), femurs were dissected from four-week-old rats, the bones were cut and the marrow extruded using a needle and a syringe. Bone marrow cells were plated in tissue culture flasks containing Eagle medium (DMEM; Gibco, Paisley, Scotland) added with 100 U/ml penicillin and 100 U/ml streptomycin. The cells were detached from the flasks by incubation with 0.25% trypsin, and after six to ten passages the cells in suspensions were implanted into rats.

D3 ESCs (paper V), a commercially available cell line (Doetchman et al. 1985) were transfected using the electroporation method with the pEGFP-C1 vector. Transfected cells were selected, cloned and termed eGFP ESCs. Thereafter, the

cells were grown in Eagle medium supplemented with 20% foetal calf serum (PAA Laboratories GmbH, Linz, Austria), 0.1 mM 2-mecraptoethanol (Sigma, St. Louis, MO), 1% nonessential amino acid stock (Gibco), 100 U/ml penicillin and 100 U/ml streptomycin and 1,000 U/ml recombinant mouse leukaemia inhibitory factor (LIF; Chemicon International Temecula, CA). Neuronal differentiation was induced by culturing, eGFP ESCs in serum containing Eagle medium without LIF for two days and then transferring the cells into serum-free medium supplemented with insulin, transferrin, selenium and fibronectin. On the eighth day of differentiation the eGFP ESCs were transplanted into rats.

IRON-OXIDE AND BrdU LABELLING

Before transplantation, superparamagnetic iron-oxide nanoparticles were added to the cell cultures. Endorem®, (Guerbet, France), which was chosen for labelling, is a commercially available contrast agent based on dextran-coated iron-oxide nanoparticles. It is available as an aqueous colloid and has been approved for human use. Five days before transplantation, Endorem® was added to a culture of MSCs (10 µl/ml culture medium) (papers IV, V). After 72 h the contrast agent was washed out. At 24 h before transplantation, the MSCs were co-labelled with 5 µM bromodeoxyuridine (BrdU) (papers IV, V). The eGFP ESCs were labelled with 112.4 mg/ml Endorem® added to the culture medium in three passages (paper V).

GRAFTING OF STEM CELLS

Nanoparticle-labelled MSCs or eGFP ESCs were, after lesioning, grafted into the rats either directly into the brains or injected into the femoral vein. For direct injection into the brain, following a cortical lesion, a burr hole (1 mm) was made to expose the dura on the contralateral side. MSCs, 3 x 10^5 in 3 µl phosphate buffered saline (PBS) or 2 x 10^5 in 5 µl PBS, were injected at post-lesion times 24 h (paper IV) or seven days (paper V), respectively. The injection was done slowly over a ten-minute period into the contralateral hemisphere. eGFP ESCs induced into neuronal differentiation were injected in the same way at seven days post-lesion (paper V). Thereafter, the opening was closed by bone wax and the skin sutured.

For intravenous injection after a cortical or spinal cord lesion, (papers IV, V), approximately 2 x 10^6 undifferentiated MSCs or eGFP ESCs in 0.5 ml PBS were injected into the femoral vein.

Magnetic resonance imaging (papers I, IV, V, VI)

MR recordings were made using a 4.7 T, Biospec Avance Bruker Spectrometer 47/40 (Stockholm) and Biospec Avance Bruker Spectrometer 47/20 (Prague), equipped with either a 12 cm self-shielded gradient coil, a home-made surface coil or a whole-body resonator. Images were obtained from a standard set of maps, namely ADC_W-, T_2- and PD maps. ADC_W maps provided information about changes in extra- and intracellular water homeostasis. In T_2 maps the proton relaxation times were measured, which indicate the local molecular motion. To determine the number of water molecules, PD maps were calculated from the T_2 maps.

IMAGING THE BRAIN

When imaging rat brains, the magnet was equipped with a birdcage coil. Incisors and ear bars fixed the animal's head during the procedure, and coronal MR images were recorded with the following data sequences. ADC_W maps (paper I) were spin echo images along the read-out gradient direction with the sequence parameters: repetition time (TR) = 2300 ms, echo time (TE) = 29.5 ms, acquisition matrix = 256 x 128 and reconstruction matrix = 256 x 256. T_2 maps (paper I) were obtained by multiecho sequences with the following parameters: TR = 2655 ms, TE = 40 or 120 ms, Field of view (FOV) = 4 cm, matrix = 256 x 256, slice thickness = 1 mm. T_2-weighted transversal images (papers IV, V) were measured by turbo spin echo sequences. Sequence parameters were TR = 2000 ms, TE = 42.5 ms, turbo factor = 4, number of acquisitions = 16, FOV = 3.5 cm, matrix = 256 x 256 and slice thickness = 0.5 mm.

IMAGING THE SPINAL CORD

MR images of the spinal cord (papers V, VI) were obtained using a whole-body resonator. The spine segments, fixed *ex vivo* in paraformaldehyde, were placed in a 50 ml polypropylene test tube and then centred within the magnet. A 3D-

gradient echo sequence was used for data acquisition. Sequence parameters were TR = 25 ms, TE = 5.1 ms and number of acquisitions = 128. 3D images were obtained with the dimensions: FOV = 6 x 3 x 2.4 cm, matrix = 256 x 128 x 96.

IMAGING IEON-OXIDE NANOPARTICLE-CONTAINING CELLS

To visualise iron-oxide in stem cells (papers IV, V), phantoms containing labelled cells were used for MR recordings. MR images were obtained with the same data sequences as used for the spinal cord measurements only with different geometry: FOV = 6 cm, matrix = 256 x 256, slice thickness = 1 mm.

Histology (papers I, III, IV, V)

The rats were transcardically perfused at a pressure of 0.3 bars, initially with 50 ml 0.1 M PBS with 500 IU heparin added at pH 7.4 and thereafter with 500 ml 4% paraformaldehyde in 0.1 M PBS at pH 7.4. The brains were rapidly removed from the skulls and stored at +4°C in fixative solution with 30% sucrose added. Coronal sections (40 μm) were cut on a Microm HM 400 low temperature microtome.

MORPHOLOGICAL CHARACTERISATION OF THE LESION

For morphological characterisation of the lesion (papers I, III), sections were cut throughout the area of the lesion (bregma –0.8 mm to 1.2 mm) and every fourth section was processed for cresyl violet (Nissl) staining. At each evaluation time point, 40-50 tissue sections were examined by light microscopy.

HISTOCHEMISTRY

To detect proliferating cells (papers III, IV, V); brain sections were incubated with antibodies against the proliferation marker BrdU. A monoclonal primary antibody was used combined with goat anti-mouse IgG and rabbit anti-mouse IgG as secondary antibodies.

To study differentiation into neurones or glial cells, the cell-type-specific markers neuronal nuclear antigen (NeuN) and glial fibrillary acidic protein (GFAP) were used. eGFP ESCs induced into neuronal differentiation was detected by GFP fluorescence. Double staining was employed to visualise in the same cell the possible co-localisation of cell-type-specific markers and BrdU or GFP.

DETECTION OF IRON_OXIDE NANOPARTICLES CONTAINING CELLS

Iron-oxide labelled MSCs and eGFP ESCs (papers IV, V) were detected in tissue sections by staining for iron to produce ferric Ferro cyanide (Prussian blue). Also, MRI and EM confirmed the presence of iron-oxide inside cultured cells. Transplanted iron-oxide labelled cells were detected *in vivo* by MRI.

Electron microscopy (papers I-VI)

For electron microscopy the rats were transcardically perfused at a pressure of 0.3 bars, initially with 50 ml 0.1 M PBS with 500 IU heparin added at pH 7.4 and thereafter with 500 ml 3.0% glutaraldehyde in 0.1 M PBS at pH 7.4 as a fixative solution. Immediately after the perfusion the brains (papers I, II) and the spinal cords (paper VI) were dissected and stored over night at +4°C in the fixative. Glutaraldehyde fixation was followed by post-fixation in 1% osmium tetroxide in PBS for two hours.

Cultured stem cells and vibratome sections from lesioned brains (papers III, IV, V) were fixed at +4°C in 2.5% glutaraldehyde in 0.1 M PBS at pH 7.4, followed by post-fixation for two hours in 1% osmium tetroxide in PBS.

TISSUE SAMPLING

Tissue samples (papers I, II, VI); were taken at 0.5, 1, 3, 6, 12, 24, 48 and 72 h post-lesion according to standardised procedures. In papers I and II, the brains were cut, supported by a fixture (Fig. 1), in two parts close to the lesion centre at bregma –0.5 mm, and the caudal cutting face was placed tightly against the fixture wall (Fig. 1b). Coronal slices (~ 1 mm thick at bregma -0.5 mm to -1.5 mm)

were placed on the fixture plate (Fig. 1a) with the brain midline aligned to the central mark. Tissue samples were selected bilaterally, according to the fixture marks, between 2 and 3 mm lateral to the midline, and subsequently these two samples were further cut into three specimens, which represented the cortical layers I-II, III-IV and V-IV, respectively. Unbiased sampling was obtained by randomised sample orientation during further EM preparation.

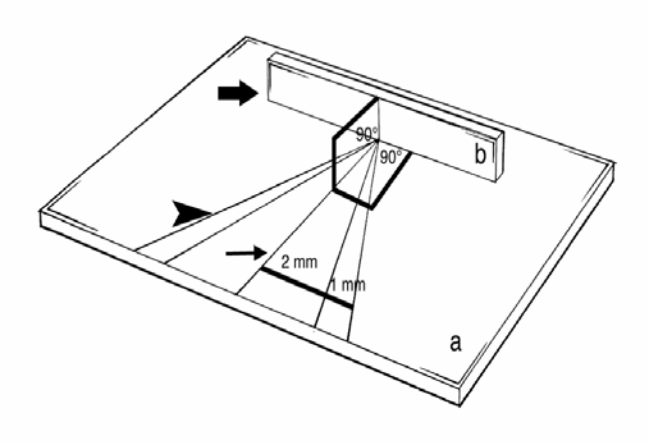

Fig. 1. A fixture made of polystyrene for standardised sample collection. On the bottom of the plate (a) a supporting wall (b, block arrow) is inclined 90°. A central mark (thin arrow) is outlined on the bottom plate at a 90° angel to the supporting wall. Bilateral help lines (arrowhead) are marked on the bottom plate in order to find the sensory motor cortex at a distance of 2 and 3 mm from the central mark.

In paper IV, the lesion centre in the spinal cord was macroscopically defined as the place where the spinal cord was thin and possible to fold. Bilaterally to the lesion centre, five 1 mm thick transversal sections were taken according to the following procedure. The first sample (C) was cut in lesion centre, as defined above; two rostral samples (A, B) were cut 0.5 and 1 cm from the lesion centre, respectively; two caudal samples (D, E) were cut 0.5 and 1 cm from the lesion centre. Thereafter the samples were prepared for EM examination.

PREPARATION FOR ELECTRON MICROSCOPY

After fixation the samples were dehydrated in increasing concentrations of ethanol, embedded in resin Agar 100 or Epon 812 and polymerised in blocks at 60°C. Semithin sections (1 μm) (papers I, II, III, VI) were cut from the tissue samples and stained with toloudin blue. Areas of interest were selected using light microscopy (LM). Ultrathin sections (~ 60 nm) were cut from the selected areas, while the stem cell samples (papers IV, V) were cut directly from the blocks into thin sections. All cutting was done on an LKB V or Reicherts Ultracut

S ultramicrotome. The ultrathin sections were stained with the heavy metals uranyl acetate and lead citrate to obtain contrast for transmission electron microscopy.

EVALUATION PROCESS

To obtain a semi-quantitative estimation (papers I, II, VI), we developed standardised evaluation protocols considering both quantitative and qualitative parameters. The evaluation was based on the following structural parameters: nuclear condensation, chromatin clumping or margination, cytoplasm condensation and vacuolisation, organelle changes and nuclear and plasma membrane "blebbing" and rupture as well as honeycomb vesicles and disperse lamellae in myelinated axons. The evaluation also included the counting of different cells. The section areas were measured and the cell densities per mm^2 were calculated (papers I, II). Pyramid cells, interneurones, astrocytes and oligodendrocytes, affected as well as unaffected, were separately counted. Furthermore, the status of the neuropil, considering the profile of dendrites and axons, was qualitatively evaluated.

All samples were examined using Zeiss CEM 900 and Philips Morgagni 268D transmission electron microscopes. Electron micrographs were made of areas of interest, and the final evaluation was made from these micrographs.

RESULTS

For a detailed description of the results, see appended publications and manuscripts. Here, the results are summarised as follows:

Evaluation of lesions (papers I, VI)

The animals had the expected functional impairment at 24 h post-lesion (paper I), scoring 1 or 2 in the beam-walking test, thus indicating an adequate lesion. At 48 h and 72 h the beam walking score was 3 or 4, which indicated functional improvement.

Following the cortical photochemical lesion (paper I), MRI showed reduced ADC_W values in the lesion area at 0.5–6 h, (Fig. 2a-b) while T_2 maps showed increased relaxation times (Fig. 2e-h). The corpus callosum and the external capsule were found as bright areas in ADC_W and T_2 maps, starting at 6 h (Fig. 2c, g) and becoming more pronounced at 24 h (Fig. 2d, h). A brain midline shift towards the contralateral hemisphere was observed at 3 h in ADC_W maps (Fig. 2b) as well as in PD maps (Fig. 2k) and at 6 h in T_2 maps (Fig. 2g). No changes were observed by MRI in the contralateral hemisphere.

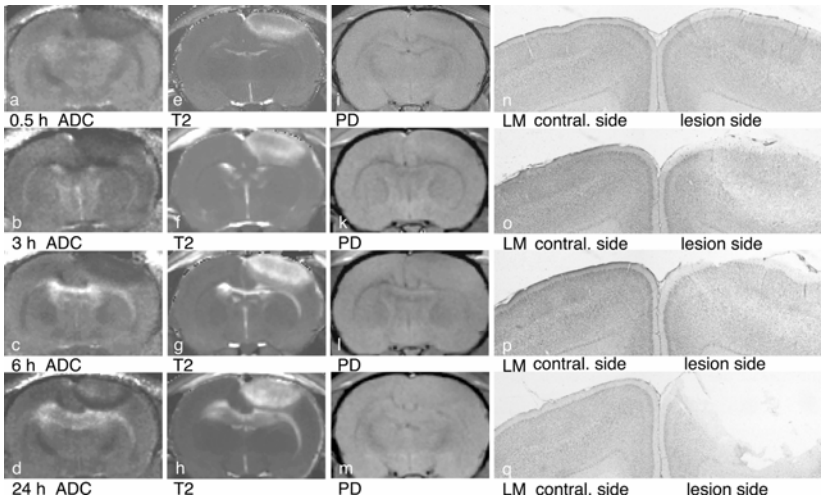

Fig. 2. MR images (ADC_W, T_2 and PD maps) showing coronal sections of lesioned brains, and Nissl stained brain sections from the contralateral and lesioned cortex at 0.5, 3, 6 and 24 h postlesion, following a cortical photo-chemical lesion. In ADC_W maps, reduced values are seen as dark areas in the lesion (a–d), and in T_2 increased values are seen as hyper intense areas (e–h). At 6 h and 24 h, the corpus callosum was observed as hyper intense areas in ADC_W maps (c–d) and T_2 maps (g–h). In PD maps midline shifts are observed in (k–l). In Nissl sections, tissue in the lesioned area can be seen to gradually disintegrate between 0.5–24 h (n–q).

Following the spinal cord compression lesion (paper VI) hypo intense areas were found at the sites of injury. The hypo intense signal was mainly caused by haemorrhages, which is the consequence of the grey and white matter disintegration. Hyper intense regions surrounded hypo intense areas, and this gave us the possible to evaluate the lesion appearance. The lesion extent in the longitudinal spine axis was at its maximum at 0.5 h post-lesion and was thereafter diminished within 6 hours. At 48 h some hypo intense signals were observed.

Time course of ultrastructural changes in cortical neurones (papers I, II)

Electron microscopy showed in control tissue a normal profile of myelinated axons, axon terminals and dendrites (Fig. 3a). Homogeneously distributed nuclear chromatin, distinct mitochondria cristae and distinctly double-lined nuclear and plasma membranes (Fig. 3b) were present as previously described (Cragg 1976). After evaluating all of the experimental samples, ultrastructural features were used to define three categories of damaged neurones, as follows:

- ”Electron dense neurones” (EDN): highly electron dense nerve cells with condensed nuclei. Nuclear chromatin appeared clumped or marginated. In the vacuolated cytoplasm, dense organelles were occasionally visible, and the nuclear and plasma membranes were intact (Fig. 3c).
- ”Electron weak neurones” (EWN): nerve cells with enlarged round nuclei. The diluted cytoplasm showed peripheral clearing. Expanded or normal organelles were clustered around the nuclei. Nuclear chromatin appeared flocculent with some margination, and the nuclear as well as plasma membranes were intact (Fig. 3d).
- Apoptotic cells with clumped chromatin and highly vacuolated cytoplasm (Fig. 3e-f).

We characterised these cells, counted them and calculated the cell densities on the ipsilateral and contralateral sides in both lesion models at each post-lesion time point.

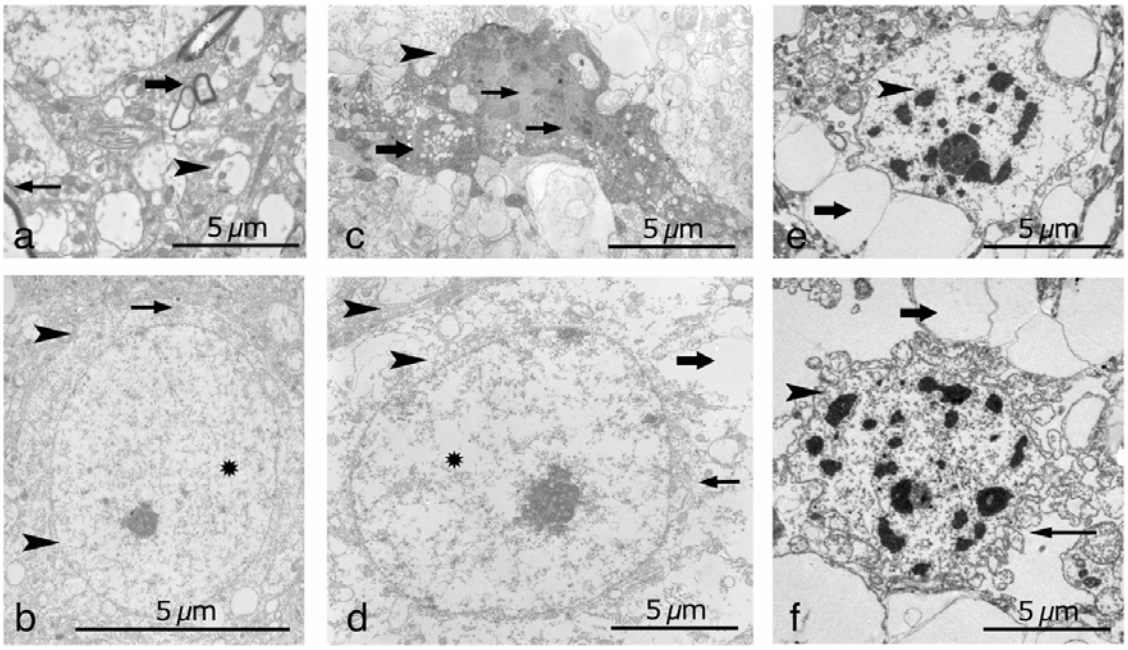

Fig. 3. Electron micrographs showing control tissue and different cell types in lesioned tissue. In control tissue the neuropil (a) showed a normal profile of myelinated axons (block arrow), dendrites (arrowhead) and axon terminals (thin arrow). Cells contained oval-shaped nuclei with homogeneously distributed chromatin (asterisk), distinct organelles (thin arrow) and intact membranes (arrowheads), as shown in b. EDN cells (c) contained clumped chromatin (thin arrows) and cytoplasm vacuoles (block arrow) and intact membranes (arrowhead). EWN cells (d) with large round nuclei contained slightly disorganised chromatin (asterisk). Peripheral cytoplasm clearing (block arrow) and clustered organelles (thin arrow) around the nucleus are visible. The membranes are intact (arrowheads). In e and f, apoptotic cells with clumped chromatin (arrowheads) and cytoplasm vacuoles (block arrows) are shown. Membrane "blebbing" (thin arrow) is prominent in f.

CELL DENSITIES

EDN and EWN cells were found in both hemispheres after a photochemical lesion, while apoptotic cells were most prominent following compression lesioning. There was no marked difference between the cell densities in layers IV and V, therefore only the densities in layer V are presented.

Cortical photochemical lesion

The cell density in the lesioned area (Fig. 4A) was 11.93, 10.56, and 18.36 cells/mm^2, at 0.5, 1, and 3 h post-lesion, respectively. At 6 h the tissue was disintegrated and therefore was not evaluated. Compared with 218.92 cells/mm^2 in control tissue, the cell density on the contralateral side (Fig. 4B) decreased from 218.82 cells/mm^2 at 0.5 h to 177.36 cells/mm^2 at 6 h. At 12, 24, 48, and 72 h, the cell density was 120.99, 131.78, 82.29 and 118.27 cells/mm^2. EWN cell density in total decreased from 173.03 cells/mm^2 at 0.5 h to 10.43 cells/mm^2 at 6 h, while EDN cell density increased from 10.18 cells/mm^2 to 36.52 cells/mm^2 at the same time points. At 12–72 h a mixed cell population was present.

Cortical compression lesion

The cell densities following compression lesion showed no marked differences between the lesioned area (Fig. 4C) and the contralateral side. (Fig. 4D). Compared with 212.50 cells/mm^2 in control tissue, total cell density in the lesioned area (Fig. 4C) decreased from 135.20 cells/mm^2 at 0.5 h to 105.32 cells/mm^2 at 12 h. At the same time points, the density of apoptotic cells increased from 5.00 cells/mm^2 to 49.88 cells/mm^2. At 12 h, apoptotic cells were found most frequently: being 47.3% of total cell number. On the contralateral side (Fig. 4D) the total cell density decreased from 134.46 cells/mm^2 at 0.5 h to 104.56 cells/mm^2 at 12 h, while the density of apoptotic cells increased from 4.98 cells/mm^2 at 0.5 h to the highest density of 21.48 cells/mm^2 at 24 h.

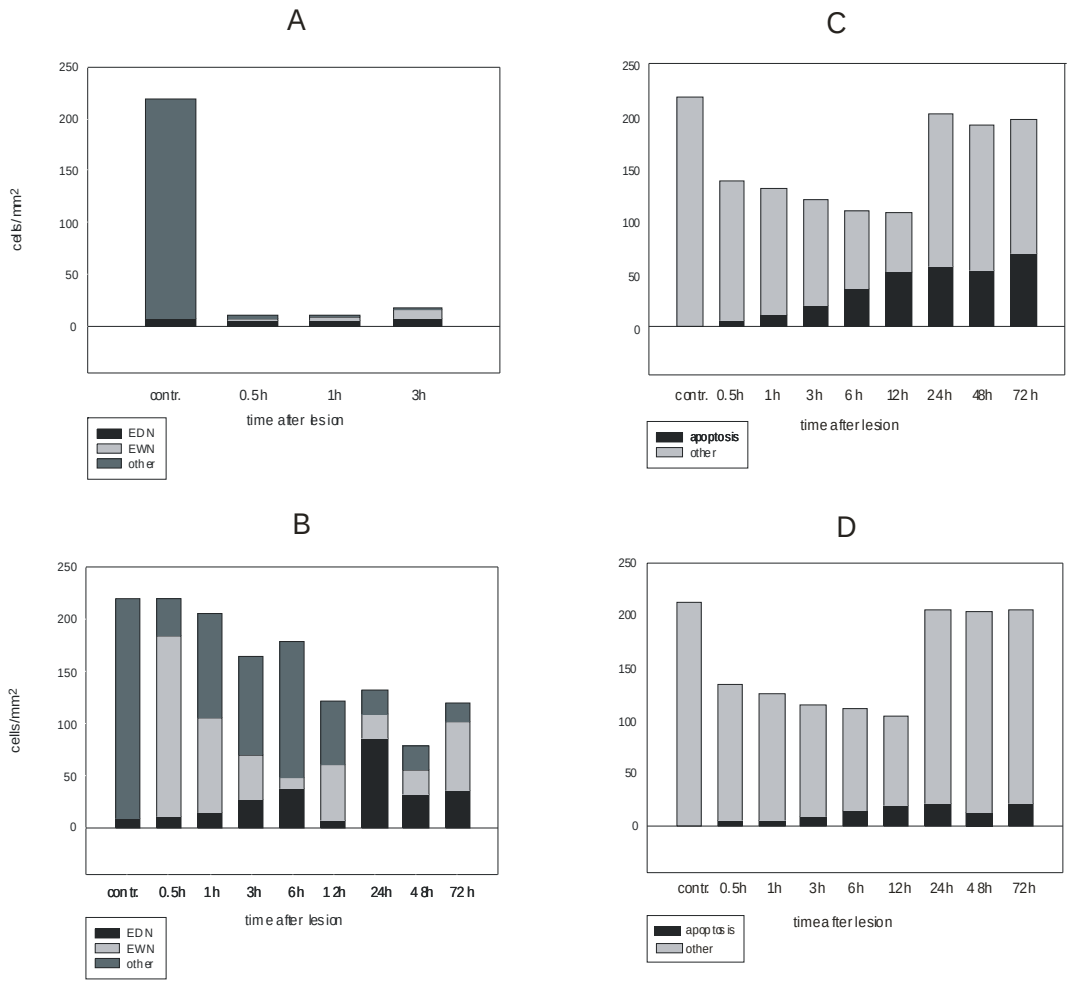

Fig. 4. Stacked column graphs, in which are shown cell densities of EDN, EWN and apoptotic cells plus the densities of remaining cells in the tissue. In Fig. 4A, showing cell densities following a cortical photochemical lesion, a mixed cell population was found in control tissue. Compared with control tissue, highly decreased cell densities were found at 0.5, 1 and 3 h post-lesion. In Fig. 4B shows cell densities on the contralateral side are shown. At 0.5 h, the EWN cell is the dominant cell type. EWN cells decrease in number at 1-3 h but remain a frequent cell type throughout all recorded time points. Following a cortical compression lesion (Fig. 4C) no apoptosis was found in control tissue. Compared with control tissue, total cell densities in the lesioned area were decreased at 0.5-12 h. At 12 h, approximately half of the total cell number was apoptotic cells. In Fig. 4D, cell densities on the contralateral side are shown with decreased numbers of total cell densities at 0.5–12 h.

ULTRASTRUCTURE

Electron microscopy showed that a cortical photochemical lesion resulted in a permanent infarction and a cortical compression lesion in a *penumbra* zone.

Cortical photochemical lesion

Already at 0.5 h, the ultrastructure in the lesioned area appeared disorganised (Fig. 5a). Although the neuropil was severely affected with swollen dendrites and large extracellular vacuoles (Fig. 5b), individual cell bodies were easily identified as separate entities (Fig 5c-d). Most cells showed varying degrees of cytoplasm condensation and chromatin margination, and cells with signs of apoptotic (Fig. 5c) as well as necrotic (Fig. 5d) cell death were found.

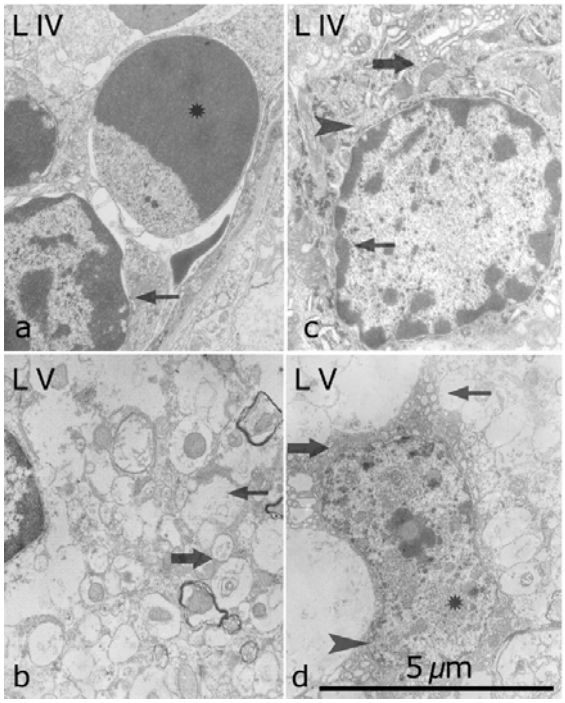

Fig. 5. Electron micrographs, in which cortical layers IV and V in the lesioned hemisphere are shown at 0.5 h post-lesion following a cortical photo-chemical lesion. Some cells with an apoptotic appearance were found already at 0.5 h, as shown in a. Within the highly disintegrated cells, a separate body, probably an apoptotic body, with clumped chromatin was present (asterisk). Marked chromatin marginations and large chromatin clumps (thin arrows) dominated the nucleus. The neuropil (b) is dis-organised with large vacuoles (thin arrow) and swollen dendrites (block arrow). Some cells appeared with distinct nuclei (c). The chromatin is marginated (thin arrow) to the double-lined nuclear membrane (arrowhead) and organelles (block arrow) are possible to identify within the disorganised cytoplasm. In some cells the nucleus is identifiable as a separate unit (d) and the cell body can be outlined (thin arrow). The chromatin is electron dense and clumped (asterisk), and the nuclear envelope is in some parts observed as double-lined and in some parts ruptured (arrowhead).

In the contralateral hemisphere the ultrastructure of the neuropil was well organised at all post-lesion times. However, EDN and EWN cells were found at all time points. At each time point, additional cells with varying morphology were present. Compared to controls, most cells showed at 3 h a changed ultrastructure: marked chromatin clumping and margination were seen as well as reduced cell size (Fig. 6a, b). This gave the cells an electron dense appearance. In some of the cells ruptured nuclear membranes were found, which is one of the criteria for irreversible cell death. Diluted cytoplasm with expanded organelles and membrane "blebbings" were also seen in these cells. At 6 h the nuclear chromatin in most cells, though heterogeneously distributed, showed only slight clumping and margination, which gave the cells a less electron dense appearance (Fig. 6c, d). All membranes were intact at this time point. At 12–72 h, cells with varying ultrastructure were found together with EDN and EWN cells. Within some cells at 48 h the nuclei contained dispersed nucleoli.

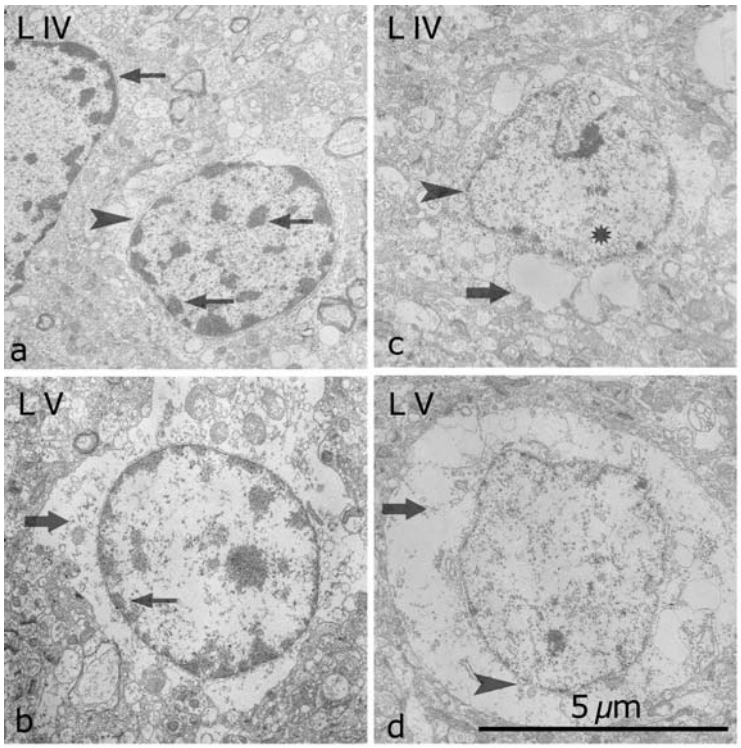

Fig. 6. Electron micro-graphs showing at 3-6 h post lesion cortical layers IV and V on the contra-lateral side following a cortical photochemical lesion. As shown in a and b, most cells at 3 h were small in size with a condensed appearance with nuclei containing highly clumped and marginated chromatin (thin arrows). The double-lined nuclear envelope had some "blebbings" and ruptures (a, arrowhead), and the cytoplasm appeared diluted (b, block arrow). At 6 h, most cells (c, d) appeared diluted with slightly disorganised and clumped chromatin (asterisk). The folded nuclear membrane in some cells was distinctly double-lined (c, arrowhead) and large cytoplasm vacuoles and swollen organelles (c, block arrow) were observed. Other cells had membranes with some "blebbings" (d, arrowhead) and the plasma compartment appeared diluted (d, block arrow) without distinct organelles.

Cortical compression lesion

Following a compression lesion, the neuropil in the lesioned area already appeared expanded at 0.5 h. Also, slightly affected cells with shrunken nuclei, cytoplasm vacuoles and expanded ER were found at 0.5 h. At 48 h marked chromatin clumps (Fig. 7a), were observed. This indicates an early stage of apoptotic cell changes. At 72 h apoptotic bodies (Fig. 7b) were found.

On the contralateral side, the neuropil was well-organised at all time points. A slightly enlarged ER was already noticed at 0.5 h and the enlargement was more pronounced at 1 h. At 3 h large stacks of ER (Fig. 7c) dominated the cytoplasm compartment in most cells, which is a sign of secondary delayed cell death.

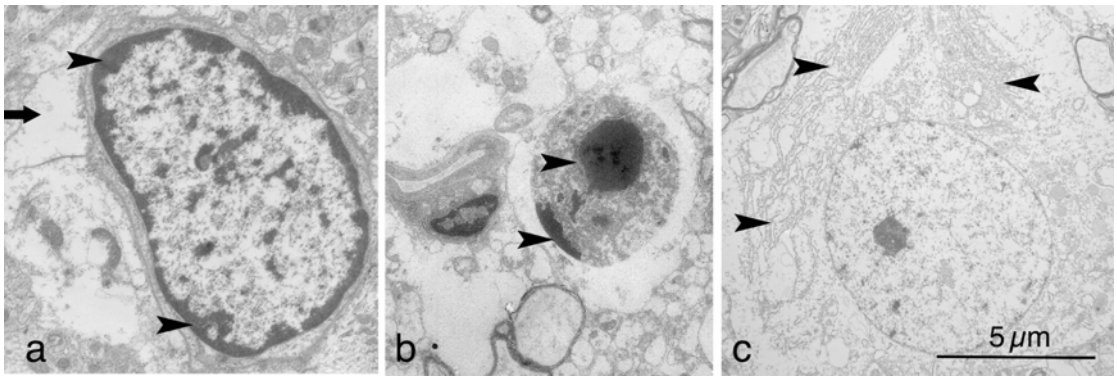

Fig. 7. Electron micrographs of apoptotic cell changes in the lesioned area, and secondary delayed cell death on the contralateral side, following a cortical compression lesion. At 48 h, marked chromatin marginations (a, arrowheads) and cytoplasm vacuoles (block arrow) were found in the lesioned area. Apoptotic bodies with large chromatin aggregations (b, arrowheads) were present at 72 h. In cells on the contralateral side, we found stacks of enlarged endoplasmatic reticulum (c, arrowheads), which is a sign of secondary cell death.

Stem cell contribution to lesion repair (papers III-V)

Following a lesion, endogenous stem cells and implanted nanoparticle-labelled stem cells migrated to the lesion site. Histochemistry detected iron-containing or dividing cells, electron microscopy confirmed nanoparticles inside the cells, and magnetic resonance imaging tracked the cell migration.

ENDOGENOUS STEM CELLS AFTER LESIONING

When studying the contribution of endogenous stem cells to tissue repair, rats were subjected to beam-walking training and fluoxetine treatment, either

separately or in combination, before lesioning. Fluoxetine is known to enhance the number of granular cell progenitors in adult rats, and after 14 days of pretreatment, cell migration to the lesion site was substantially enhanced in all rat groups.

Cortical photochemical lesion

A photochemical lesion itself induced the migration of dividing cells in the cortex and subcortical white matter surrounding the lesioned area. Five days after lesioning, the density of BrdU-positive cells was increased at the lesion site. (Fig. 8a) This was confirmed by EM, which showed some cells with two nucleoli, thus indicating dividing cells (Fig. 8b). Double staining with cell-specific neuronal and glial markers showed that 46% of BrdU-positive cells differentiated into neurones or glial cells. In pre-treated rats, the number of dividing cells was increased in all groups and in particular after fluoxetine treatment, when the number of dividing cells was increased approximately eight folds. 78-55% of the dividing cells were differentiated into neurones or glial cells.

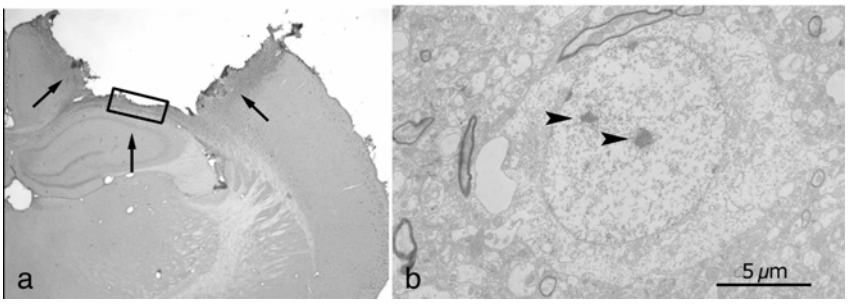

Fig. 8. A photomicrograph and an electron micrograph showing BrdU positive dividing cells at 3 h post-lesion, following a cortical photochemical lesion. The number of dividing cells (a, thin arrows) was enhanced at the lesion boarder. In the marked area (a), electron microscopy showed cells with two nucleoli (b, arrowheads), indicating eventual cell division.

IMPLANTED ADULT STEM CELLS AFTER LESIONING

Stem cells containing iron-oxide nanoparticles were visible in culture by LM, either with phase contrast or stained for iron, i.e. Prussian blue (Fig. 9a, b). EM showed clusters of iron particles inside the cells, which were incubated with nanoparticles for 48–72 h (Fig 9c, d). The clusters were surrounded by cell

membranes, which indicated endocytotic iron uptake into the cytoplasm. MSCs stained with BrdU to detect dividing cells were co-labelled with Prussian blue (Fig. 9a); BrdU-Prussian blue-positive MSCs were viable iron containing cells. The MSCs stayed viable for 10 passages.

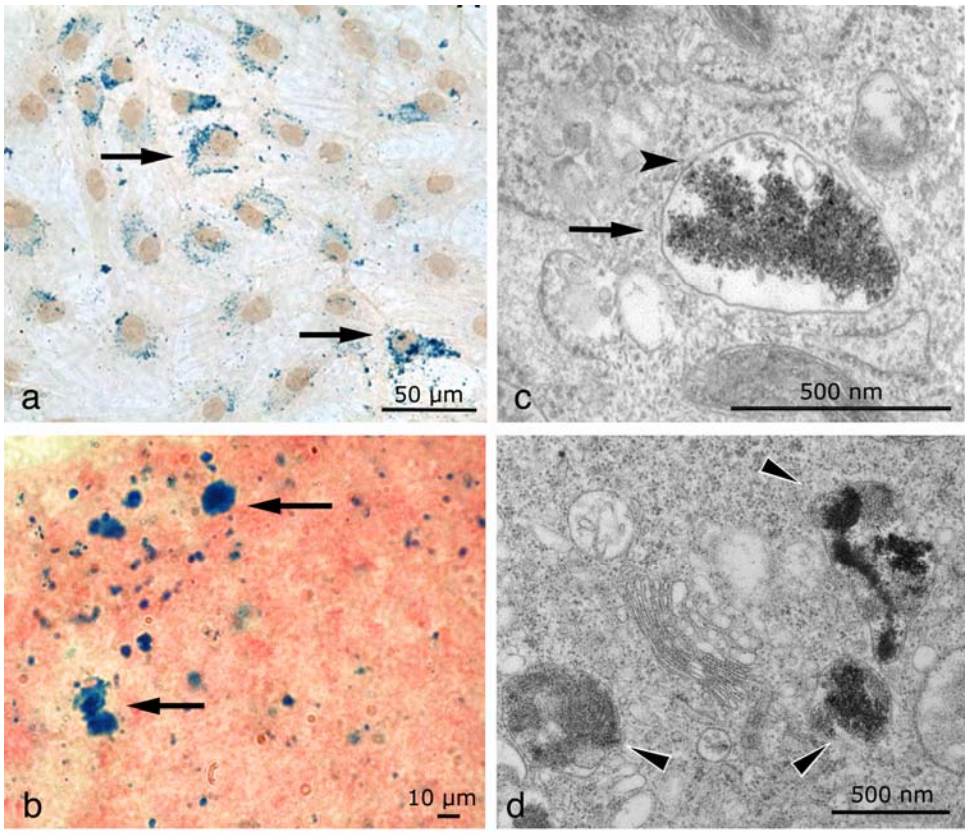

Fig. 9. Photomicrographs and electron micrographs of iron-oxide nanoparticle-labelled stem cells in culture. Prussian blue positive iron-oxide labelled cells are seen in a and b (thin arrows); MSCs in a and eGFP ESCs in b. Electron microscopy (c, d) showed clusters of nanoparticles (arrowheads), some of which were surrounded by distinct cell membranes (c, thin arrow).

Cortical photochemical lesion

Following a photochemical lesion, nanoparticle/BrdU-labelled MSCs migrated to the border zone of the lesion. Regardless of the administration route, direct injection into the contralateral brain hemisphere or intravenous injection into the femoral vein, the cell migration was substantial. Cell implants, which were grafted directly into the contralateral brain hemisphere, were immediately visible in MR images as a hypo intense signal at the injection site.

During the first days after MSC implantation into the brain, no recognisable hypo intense MR signal was detected in the lesion. Eight days after grafting, a hypo intense signal was observed in the lesioned area (Fig. 10a), which intensified during the second and third weeks. Histology confirmed that a large number of Prussian blue/BrdU-positive cells were present at the lesion border, and the intensity of the MR signal corresponded to the number of Prussian blue-positive cells. Similar MR signals were observed after the intravenous injection of MSCs (Fig.10b). The signals persisted for seven weeks.

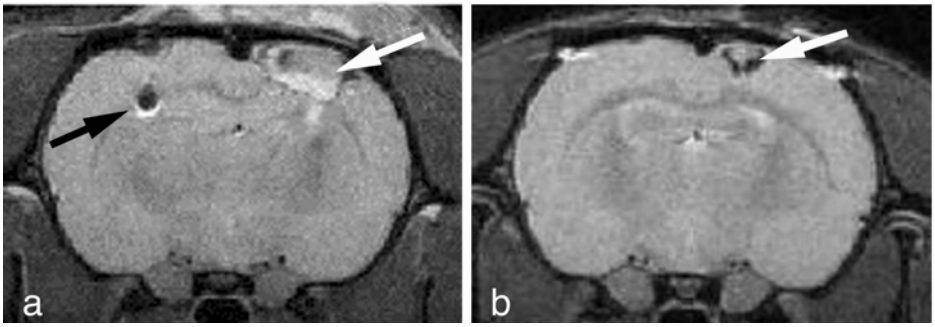

Fig. 10. MR images showing a cortical photochemical lesion and iron-containing cells. After lesioning, MSCs were implanted into the contralateral hemisphere or injected into the femoral vein. Eight days after grafting into the contalateral hemisphere a hypo intense signal (a, black arrow) at the injection site and a hyper intense signal (a, white arrow) in the lesioned area were visible. Six days following intravenous injection a hypo intense signal (b, white arrow) was observed in the lesion.

Spinal cord compression lesion

Following a balloon-compression lesion, nanoparticle labelled-MSCs were injected intravenously into the femoral vein. MRI, performed *ex vivo* four weeks after implantation, showed the lesion as a dark hypo intense area. Histology confirmed a large number of Prussian blue-positive cells in the lesioned area. The lesioned area in grafted animals appeared smaller in size in MR images, compared to controls. Since MSCs populated the lesioned area, the decreased lesion size might suggest a positive effect of MSCs on lesion repair.

IMPLANTED EMBRYONIC STEM CELLS AFTER LESIONING

Nanoparticle labelled-eGFP ESCs were co-labelled with Prussian blue and, by using LM iron was confirmed inside the cells. Counts of Prussian blue-positive ESCs revealed that the number of labelled cells increased until the third passage; thereafter, not the number of cells but the amount of iron particles inside a given individual cell increased. EM showed nanoparticle-containing eGFP ESCs in culture.

Cortical photochemical lesion

Following a photochemical lesion, the lesioned area was observed in MR images as a hyper intense area with hypo intense borders (Fig. 11a). Two weeks after direct injection of nanoparticle labelled-eGFP ESCs into the brain contralaterally to the lesion, a hypo intense signal was observed at the injection site, in the corpus callosum and in the lesion (Fig. 11b). After the intravenous injection of eGFP ESCs, a hypo intense MR signal was found only in the lesioned area and the first signal was observed one week after injection. The signal reached a maximum at two weeks and persisted for the next two weeks (Fig. 11c). At the same evaluation time points, Prussian blue/GFP-positive cells were detected in the corpus callosum as well as at the lesion border (Fig. 11d–f).

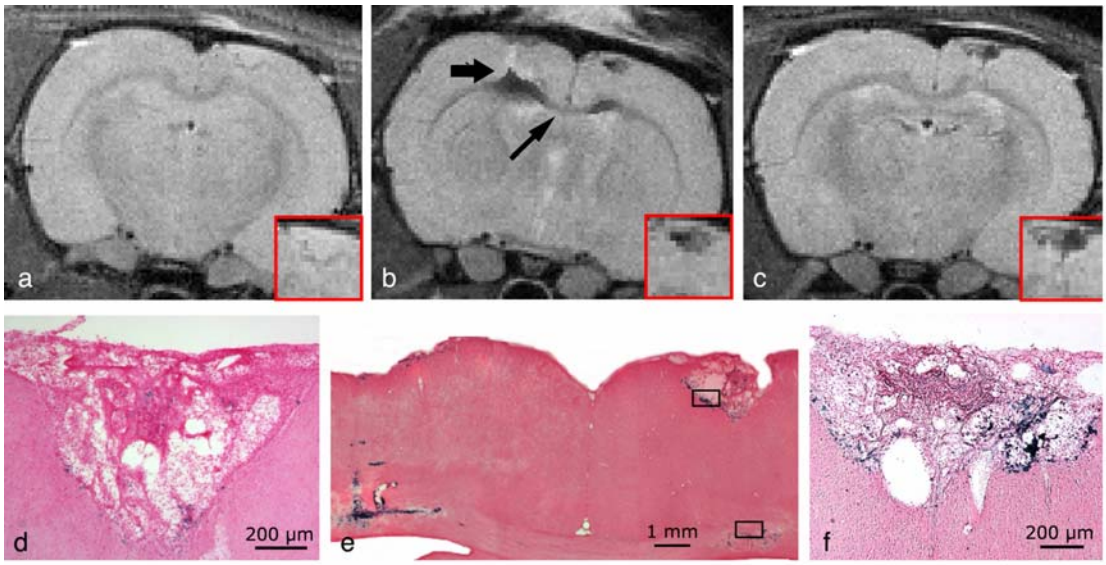

Fig. 11. MR images of a cortical photochemical lesion and iron-containing cells. Following the lesion, iron-oxide nanoparticles-labelled eGFP ESCs were implanted. Two weeks after lesioning, the lesioned area is visible as a hyper intense area with sharp hypo intense borders (a, inset). Two weeks after direct injection to the contalateral hemisphere, the cell implant (b, block arrow), the lesioned area (b, inset) and the corpus callosum (b, thin arrow) are seen as hypo intense regions. Two weeks after intravenous injection, the lesion is visible as a hypo intense signal (c, inset). After lesioning, without cell transplantation, only few Prussian blue positive, iron-containing cells were found (d). Four weeks after grafting dense Prussian blue staining was observed at the injection site, in corpus callosum and at the lesion border (e, marked areas). Four weeks after intravenous injection, a high number of Prussian blue positive cells were found at the lesion site (f).

EM showed iron-oxide nanoparticles in brain tissue samples from lesioned rats transplanted with eGFP ESCs. In lesioned brain tissue, injected with eGFP ESCs contralaterally to the lesion, dense clusters of nanoparticles were observed in cell cytoplasm. In rats injected intravenously with labelled eGFP ESCs, nanoparticles were found mostly in cells at the lesion border.

Time course of ultrastructural changes in spinal cord neurones (paper VI)

Electron microscopy showed in control tissue homogenously distributed nuclear chromatin, distinctly double-lined membranes and distinct organelles as well as well-structured axon sheaths with distinct myelin lamellae as previously described (Cragg 1976).

ULTRASTRUCTURE

In tissues taken 0.5 cm from the lesion epicentre, apoptosis of different advancements were found at 0.5-6 h post-lesion. The chromatin was highly clumped but no apoptotic bodies were seen at these time points. At 12-72 h cells with necrotic appearance were found. Periaxonal spaces were seen in axons at 0.5 h and at all evaluation time points axons with disintegrated structure were present.

DISCUSSION

Any form of injury in the central nervous system will, if it continues long enough, cause cell disruption or cell death, and focal lesions result in necrotic areas with rapidly dying cells. Since cells in this area cannot be rescued, no potential therapy other than preventing the primary injurious insult is available. There is always a gradient of hypoxia, starting from the core of the insult to the more peripheral parts of the lesion, which leads to a *penumbra* zone surrounding the area of immediate cell death. In this area cell death takes time to develop and is, consequently, possible to prevent. Ischemic tissue reveals a mixture of morphological features developing over time. However, using models that are well-defined in location and time, the time course of morphological changes can be studied with respect to a potential therapeutic window.

To study morphological changes of ischemia in the CNS, several different models have been developed in experimental animals. Global ischemia is achieved by interrupting the blood supply to the brain for a period of a few minutes, and thereby rapid cellular changes associated with the total loss of blood perfusion can be studied. To study the long term dynamics of injury and recovery, a variety of models are available. In these models, rodents are most commonly used as experimental animals, and focal lesions, mimicking either a permanent or reversible ischemic episode in one or both hemispheres, can be studied in brain tissues of the rodents. One of our aims was to study the time course of morphological changes in ischemia. To avoid a mixture of features, when studying cortical morphological changes, different severities of ischemia were studied separately in two models, namely the cortical photochemical lesion mimicking a permanent infarction and the cortical compression lesion mimicking a temporal ischemia. Since the balloon-induced compression lesion model is useful when studying secondary processes, e.g. ischemia, following spinal cord injury, we used this model to study the time course of morphological changes in spinal cord tissue.

The models

CORTICAL PHOTOCHEMICAL LESION

A cortical photochemical lesion was chosen as a model of severe cerebral ischemia. This model is different from currently used occlusion techniques, e.g. middle cerebral artery occlusion (MCAO) model, in which arteries are permanently or temporarily occluded (Moseley et al. 1990) (Garcia et al. 1993) (Garcia et al. 1995). The photochemical lesion results in an intravascular coagulation in the tissue. The light beam is focused and calibrated to a certain diameter, and only blood vessels directly hit by the light are damaged; consequently, no collateral blood circulation is present. The lesion is therefore well defined in location and size and has sharp borders between intact and lesioned tissue; that is, no *penumbra* zone is present. However, this is included in the criticisms of the lesion model. The apparent absence of a *penumbra* zone, i.e. a rescuable region, is regarded as a disadvantage. Also, the prominent vascular injury, which results in the early opening of the blood brain barrier and early vasogenic oedema, is also criticised. In this study, a photochemical lesion resulted in a permanent infarction within 3 h after lesioning, at which time point the tissue started to disintegrate and cell death, examined at the ultrastrucural level, was mostly of necrotic origin. Since a photochemical lesion is also highly reproducible, the model is useful when studying ultrastructural changes in ischemic infarction.

CORTICAL COMPRESSION LESION

A cortical compression lesion was employed to mimic short-term ischemia, resembling mild brain trauma. The lesion is assumed to mimic the *penumbra* zone around the core lesion in stroke. The MCAO technique has also been used to produce moderate ischemic brain injury. However, the MCAO lesion model, though used with only a temporary artery occlusion, results in relatively severe tissue damage, which, also due to the lack of refinement, complicates the examination of delayed cell death in the lesion. The advantage of an extradural cortical compression lesion is that the severity and duration of ischemia, and thereby also the morphological and neurological consequences, can be manipulated (Kundrotiené et al. 2002). It is known that a reduction in blood flow to 20-40% of normal levels results in delayed cell death in the brain, while a reduction to levels below 20% results in necrotic cell death (Ginsberg and Pulsinelli 1994) (Kuroda and Siesjo 1997). A cortical compression lesion, obtained

by using a 2.8 mm piston compression for 30 min, has been shown to reduce blood flow in the centre of the lesion to ~20% of normal levels during the first five minutes and thereafter to approximately 60% of normal levels (Chen 2001). At the ultrastructural level, most of the affected cells within the lesioned area showed signs of apoptosis and at 12 h after lesioning the number of apoptotic cells was 47% of the total cell number. Thus, the cortical compression lesion resulted in morphological changes characteristic for a *penumbra* zone and delayed cell death can be studied.

SPINAL CORD COMPRESSION LESION

Balloon-induced compression is a simple method to produce a lesion in the spinal cord, and the lesion model requires minimal surgical preparation. Since the balloon used for the lesioning is inserted several segments below lesion and can be inflated to a defined volume, the duration of cord compression can be regulated. Also, the precise location can be maintained manually through the catheter and therefore the model results in a well-controlled lesion. The duration of the compression was set to 5 min, which is below the threshold of sensitivity of spinal cord tissue to ischemia (Taira and Marsala 1996), thus leading to a pathogenesis in which both mechanical and vascular factors are involved, and secondary processes following injurious insults can be studied.

Cell death and tissue damage following ischemia

The biology of events following lesioning in experimental models differs from one model to another. Anoxia or ischemia does not predominantly involve unique mechanisms of cell death, but combines elements of different mechanisms such as exitotoxicity, calcium damage, metabolic disturbance, and free radical production. In particular, increasing levels of intracellular calcium is a shared property among many mechanisms. Increased intracellular calcium concentrations trigger processes leading to neuronal cell death, both apoptotic and necrotic. Also, ischemia may lead to a withdrawal of trophic factors, which subsequently may lead to apoptotic cell death.

MECHANISMS OF TISSUE DAMAGE

Damaged tissue becomes oedematous, and the oedema is both intracellular and extracellular. Intracellular oedema occurs when sodium/potassium exchange pumps are diminished in function and sodium, followed by water, enters the cell. Extracellular oedema arises when vascular permeability is increased. Using diffusion-weighted MRI, ADC_W maps show changes in water homeostasis in the intra- and extracellular spaces. Already at 0.5–24 h following a photochemical lesion, the lesioned area was observed as a hypo intense area in ADC_W maps. Oedema is present and subsequently, the architecture of the extracellular space is changed (Nicholson and Syková 1998) (Syková 2004). In T_2 maps hypo intense areas at the lesion were observed, which indicate changes in protein structure.

Following a cortical photochemical lesion, the neuropil in the lesioned area lost its integrity already in 30 min. The early tissue disorganisation can be explained by a greatly increased amount of metabolites, such as lactate, and electrolytes, released into the extracellular space (Ginsberg 1990). Glial cells, also damaged early in the lesion, have been proposed to have disturbed metabolism following injury (Kraig and Chesler 1990). Therefore, their endocytotic functions are diminished, resulting in an increase of metabolites in the extracellular space. This excess of metabolites leads to a more acid extracellular pH, the functional loss of membrane ion pumps (Chesler 1990) and cellular swelling (Syková 1997) (Syková and Chvatal 2000). As a consequence, cell homeostasis will be greatly changed followed by metabolic disturbances, e.g. decreased protein synthesis, and therefore, the cell structure loses its integrity at a later time point. This was also confirmed by EM, since cells were easily identified as separates entities in the lesioned area, while the neuropil lost its integrity. The severe structural changes in the neuropil were observed only at the ultrastructural level.

MECHANISMS OF CELL DEATH

In ischemic nervous tissue, exicitotoxocity contributes significantly, within some hours, to neuronal cell death (Choi 1992). The process has been described as an “osmotic explosion” (Rothman and Olney 1987). The excitotoxic cascade starts when glutamate is released from damaged astrocytes. Under normal conditions glutamate uptake by astrocytes from the extracellular space requires energy. As the ATP levels are low in ischemic tissue, the functioning of ion exchange pumps is slowed, the transmembrane sodium/potassium concentration gradient reduced

and the membrane potential diminished. All this leads to intracellular acidification and reduced glutamate uptake (Judd et al. 1996). The increased extracellular glutamate levels depolarise neurones to the extent that they fire action potentials, which lead to more glutamate release (Lee et al. 1999). Because of the extracellular glutamate excess, NMDA channels stay open, thus increasing the intracellular calcium concentration. Also, sodium and water enter the cell and cells swell. The increased calcium levels activate degradative enzymes, which contribute to the degeneration of intracellular organelles and pycnosis of cell nuclei. These events lead to cell necrosis. The excitotoxic cascade has also been shown to contribute to signalling pathways for apoptotic cell death (Fawcett et al. 2001). Following a cortical photochemical lesion, the rapid necrotic as well as apoptotic cell death in the lesioned area might be due to excitotoxicity.

As the excitotoxic cascade induces rapid cell damage within 30 min, signs of apoptotic cell death found at later time points might be induced by other mechanisms. Cells with apoptotic changes were found most frequently at 12 h, in the lesioned area, following a cortical compression lesion. Apoptosis can be initiated by a large number of different stimuli, and many conditions during ischemia offer such stimuli; free radical generation, NO production, reduced mitochondrial membrane potential, increased intracellular calcium levels, activation of calpain and increased expression of the protein p53 (Sugawara and Chan 2003) (Duchen 2000) (Yang and Xue 2004). Also, the withdrawal of trophic factors, e.g. neurotrophins, has been proposed to cause apoptosis, not only during development but also during injury (Campenot and MacInnis 2004) (Chen et al. 2002). Since the presence of appropriate trophic factors much improves the ability of a cell to survive a stressful situation, the withdrawal of neurotrophins could cause cell damage and subsequently cell death. The morphological features of apoptotic cells following a cortical compression lesion did not fully fit into any of the three types of apoptosis described earlier, following injury in the nervous system. The nuclear changes, with chromatin aggregations, were strongly associated with apoptosis, but the nucleus was not pycnotic. The cytoplasm was highly vacuolated, but no dilation of the mitochondria or endoplasmatic reticulum was found. The cell changes in the present studies resemble those seen in type two apoptosis. It is widely accepted that large autophagic vacuoles within the cytoplasm are present in apoptotic cell death during ischemia (Lipton 1999) (Fawcett et al. 2001). Furthermore, autophagocytotic cell death, with a condensed cytoplasm containing large vacuoles and autophagocytomes, is described as a separate type of cell death in ischemia (Marzella and Glaumann 1981). This cell

death is similar to type two apoptotic cell death. The damaged cells following a cortical compression lesion, with irregularly clumped chromatin and cytoplasm vacuoles in the lesioned area, were therefore considered to be apoptotic. Importantly, there are similarities in the ultrastructural criteria of necrosis and apoptosis. Cell membrane "blebbing", swollen mitochondria and cytoplasm condensation combined with vacuolisation occur in both forms of cell death (Studzinski 1999), which complicates the characterisation of cell death. Although the nuclear morphology of apoptosis in ischemia is well described, the morphological changes in the cytoplasm have not yet been completely investigated.

CELL CHANGES ON THE CONTRALATERAL SIDES

Following a cortical photochemical lesion, EM revealed that the most frequent cells in the contralateral hemisphere at 3 h showed membrane ruptures, which is a sign of irreversible cell death. Subsequently, the changes could represent the ultimate stage in a fast death process starting already at 0.5 h. Although slightly electron dense, the cells showed neither a condensed morphology nor mitochondria with flocculent densities, which are the main criteria of irreversible cell death (Garcia et al. 1978) (Ghadially 1975). Therefore, the most frequent cells at 3 h were not considered as dying cells but as highly affected but still viable cells.

At 6 h no cells showed signs of irreversible cell death. Since the EDN cells, defined as condensed but not dying cells, were increased in number at 6 h, some electron dense cells at 3 h might have changed in structure and been identified as EDN cells at 6 h. The cells at 3 h, with irregularly clumped chromatin and condensed cytoplasm, were similar to ICC neurones. The characteristics of ICC neurones, which are pycnosis and cytoplasm shrinkage, fit into the definition of EDN cells in the present study. In earlier studies of ischemia, ICC neurones, in spite of their triangular condensed appearance, were not associated with cell death (Brown and Brierly 1972) (Brown 1977) (Petito and Pulsinelli 1984). Furthermore, in hypoglycaemic brain damage, "dark" neurones are compatible with cell survival (Auer et al. 1985a) (Auer et al. 1985b). Therefore, some electron dense cells at 3 h might survive as EDN cells at 6 h. The most frequent cells at 6 h, with irregular nuclei and a diluted cytoplasm, were similar to EWN cells, although smaller in size. As EWN cells probably are metabolically active cells, the dominant cell type at 6 h was considered to be an active viable cell. Thus,

most cells at 6 h seemed to be viable, although the most frequent cells at 3 h were highly affected. These findings indicate a breakpoint for death versus survival.

Following a cortical compression lesion, massive ER stacks was found in cells at 3 h on the contralateral side. These changes are known to occur after transient global ischemia (Kirino and Sano 1984) and are hallmarks for secondary delayed cell death. After three days there was less enlargement of the ER and the formation of large vacuoles and autophagocytomes. The large vacuoles may arise from the expanded ER, while autophagocytomes, with increased lysosomal protease activity, are fusion products of lysosomes (Nitatori et al. 1995). The presence of these elements, involved in protein break-down, indicates autophagocytosis, which leads the cell to self-destruct. This type of cell death is seen in developmental tissue, and there is also evidence for autophagocytosis after ischemia (Marzella and Glaumann 1981). Following a cortical compression lesion, only an expanded ER was found at 3 h on the contralateral side, and no indication of the formation of vacuoles was seen. However, the present study was not designed to examine longer survival times than three days.

The injury response on the contralateral sides might be due to a failure in synaptic as well as extra synaptic "volume" transmission, i.e. the movement of neuroactive substances through the volume of the extracellular space (Nicholson and Syková 1998) (Syková 1997). This information processing (Fuxe and Agnati 1991) is probably damaged at 12-24 h (Mazel et al. 2002) resulting in injured cells. Following a cortical photochemical lesion, the total cell densities on the contralateral side at 12-72 h (Fig. 4) were reduced, suggesting an increased extracellular space, which has also been confirmed by MRI (Vorisek et al. 2002). Starting at 6 h, the corpus callosum and external capsulae were observed as hyper intense areas on ADC_W and T_2 maps, thus showing increased water movement between both hemispheres. However, MRI did not detect structural changes on the contralateral side (Vorisek et al. 2002), due to relatively small MRI resolution while electron microscopy showed distinct morphological changes.

TIME WINDOWS IN ISCHEMIA EVOKED DAMAGE

After lesioning, EM showed that necrosis was complete in the core of the infarction at 3 h, followed by total tissue disintegration. Therefore, tissue samples were not possible to evaluate after 3 h. Signs of irreversible cell death were found on the contralateral sides also at 3 h, and at 6 h the cells showed no

structural changes associated with cell death. Contralateral to the *penumbra* zone, the ultrastructural criteria for secondary cell death were observed only at one time point after lesioning, namely at 3 h. However, at this time point apoptotic cells were present in the contralateral hemisphere as they also were in the *penumbra* zone. Given our findings of complete cell death in the infarction and the ultrastructural criteria of irreversible or secondary delayed cell death on the contralateral side at 3 h after lesioning, we suggest 3 h to be a breakpoint at which cells either progress towards lethal changes or recover.

The threshold at which some cells undergo lethal changes and others recover depends on the individual cell's metabolic status at each time point (Collins 1989). The ATP levels within some of the cells are probably restored at 6 h after lesioning. ATP-dependent membrane pumps, such as the sodium/potassium and calcium/hydrogen exchange pumps function optimally when supplied with enough ATP. Subsequently, the membrane potential and cell homeostasis is maintained and the cell survives. Therefore, there is a possibility for neuronal reorganisation after 6 h.

The apoptotic cell death found in the *penumbra* zone in the present study was most frequent at 12 h (47.3% of total cell density) following a cortical compression lesion. Previous studies of the temporal profiles of apoptotic-like changes have shown that apoptotic cells were greatest in number 24 h following a controlled cortical impact injury in the rat cortex (Newcomb et al. 1999). It has been speculated that the biomechanical features of different compression lesion models may influence the frequency and regional distribution of apoptotic cell death (Bonfoco et al. 1995) (Choi 1996), and the compression of the cortex in the earlier studies was less than in the present study. Other differences between the previous time course studies of apoptosis and the present one are that only cell number, not cell density, was reported and that the evaluation was done by histochemistry and not by EM, with which the ultrastuctural criteria for apoptosis can be identified. However, regardless of the compression models, it is clear that there is a time delay in cell death in the *penumbra* zone compared to the core of the infarction and that the cell death is mostly apoptotic. Apoptosis occurred at low frequency already at 0.5 h, peaked at 12–24 h and continued for 48–72 h. This time delay in cell death opens the possibility for therapeutic interventions. As the apoptotic cascade is regulated by genes and associated proteins known as caspases (MacManus and Linnik 1997), caspase inhibitors would be a potential anti-apoptotic treatment. It has also been shown that

caspase inhibitors protect against apoptotic cell death in a number of *in vivo* models of neurological diseases and also against the slow neuronal death induced by ischemia (Himi et al. 1998).

Stem cell contribution to tissue repair

In most tissues a continuous turnover of cells by death and replacement is the norm rather than the exception. Cell replacement and tissue repair can be achieved in two ways. Following damage, the division of adjacent healthy cells can replace the damaged cells; that is, a mature cell divides to produce two similar copies, one of which dies through apoptosis. A second possibility occurs when a resting population of stem cells divides and some of the progenitor cells differentiate to mature cells and replace damaged cells. Different from this endogenous cell generation, the transplantation of stem cells into the tissue would be a third possibility. In the present work, the contribution of stem cells to tissue repair was studied in regard to the generation of endogenous stem cells as well as the transplantation of embryonic stem cells and bone marrow stromal cells.

Embryonic stem cells are considered to be pluripotent as they can develop into any of the tissues in the body. The discovery that embryonic stem cells can be isolated and cultured with the potential to develop into any tissue was a major medical breakthrough. As long as they are cultured under specific conditions, the cells stay undifferentiated, but they differentiate spontaneously without certain controls. Therefore, through the reliable control of differentiation specific types of cells could be achieved grown in culture, and these cells may become the basis of therapies for many serious diseases, among them neurological disorders. Endogenous stem cells, e.g. adult or somatic stem cells, have been found in more tissues than once was believed, among others in the brain and the spinal cord. Adult stem cells are undifferentiated cells found among differentiated cells in tissues and have the ability to renew themselves. Their primary role is to repair tissue and maintain cell homeostasis within the tissue in which they are found. Certain adult stem cells seem to have the capability to differentiate into a number of different cells types, given the right conditions. In the bone marrow, haematopoietic stem cells form all types of blood cells, and bone marrow stromal cells generate bone, cartilage, fat and fibrous connective tissue. Also, in the brain, regions with dividing cells that become neurones are present. The SVZ lining the lateral ventricles and the SGZ of dentate gyrus are such areas. If isolated and

cultured under controlled conditions, these stem cells might also serve as a basis for cell therapy. Endogenous stem cells may also provide an alternative to transplantation. Stimulating resident stem cells to replace dying cells could help to overcome the limitations of transplantation.

NEUROGENESIS

Following a cortical photochemical lesion, dividing cells were found in the border of the lesion. Persistent neurogenesis in the adult brain has originally been thought to occur in only a few restricted areas. The subventricular zone lining the lateral ventricles and the subgranular zone of the dentate gyrus are regarded as the main regions for stem cell generation, but other areas such as the olfactory bulb and ganglionic eminences (Pleasure et al. 2000) have also been suggested to produce precursors. The precursor cells in these zones migrate and end up in new regions as new neurones or glial cells. Furthermore, recent studies have demonstrated that the production of new neurones occurs in many different parts of the adult brain, although at a low frequency (Rietze et al. 2000) (Pencea et al. 2001) (Gould and Gross 2002). In the present study, after lesioning, the density of dividing cells was substantially increased at the lesion border in the subcortical white mater, which is situated in the vicinity of the lateral ventricle. This might indicate a progenitor migration from the SVZ to the lesion site. Following fluoxetine pre-treatment, an increased density of dividing cells was found in the lateral cortex. As fluoxetine is known to increase the concentration of serotonin by blocking its uptake, we suggest that fluoxetine acts as a paracrine secretory molecule and provokes the proliferation and migration of stem cells to the cortex from the ganglionic eminence. Beam-walking pre-treatment also enhanced the number of dividing cells in the vicinity of the lesion. Following the same model of a cortical photochemical lesion, functional recovery has been demonstrated in rats (Abo et al. 2001), and thus the functional improvement, as demonstrated by beam-walking ability, could be explained by tissue repair, including the generation and migration of new cells to the lesion. Also, EM, which showed some cells with dispersed nucleoli, might confirm the migration of new cells to the lesion border. In the interphase of stem cells and dividing cells, increased DNA transcription within the nucleoli is associated with an altered distribution of the heterochromatin and changed ultrastructure. This is manifested at the ultrastructural level as changes in the size and number of nucleoli (Leitch 2000). Thus, the EM findings might indicate cell division and reorganisation (Alberts 1989).

STEM CELL TRANSPLANTATION

Embryonic stem cells and bone marrow stromal cells have been successfully used in cell therapies in animal models, and ESCs and MSCs were transplanted into rats in the present studies.

Large numbers of ESCs can be easily cultured and transplanted into animals, and the differentiation of ESCs has been studied with some promising results. Glial precursors derived from mouse ESCs and transplanted into rats with myelin disease produce myelin in the brain and spinal cord (Brustle et al. 1999). Retionic acid-treated embryoid bodies from mouse ESCs, transplanted into the spinal cord after lesioning, differentiated into astrocytes, oligodendrocytes and neurones thus promoting recovery (McDonald et al. 1999) (Björklund et al. 2002). However, there is a lack of information about the behaviour of transplanted embryonic stem cells in the host organism, and transplantation from a donor could result in the rejection of the transplant.

Bone marrow cells may have some advantages over the use of other stem cells. They are relatively easy to isolate and culture and they have already been approved as cell therapy treatment in haematopoietic diseases. MSCs have also been shown to migrate to a photochemical lesion (Lu et al. 2001) and the transplanted animals showed an improved neurological outcome in behavioural tests (Hofstetter et al. 2002) (Li et al. 2000) (Lu et al. 2001). The usefulness of stem cells' contribution to tissue repair does not necessarily rest on the replacement of lost cell populations. Bone marrow cells secret interleukins and other regulatory molecules (Eaves et al. 1991) (Maysinger et al. 1996) that are growth factors in the CNS. MSCs implanted into the CNS could therefore stimulate tissue regeneration and improve neurological outcome by other mechanisms than direct neuronal replacement (Hofstetter et al. 2002) (Li et al. 2000) (Lu et al. 2001).

To study the fate of implanted stem cells in the host organisms, it would be of benefit to find a suitable marker approved for human use. This would open new possibilities for using and studying stem cells in human medicine. Several groups have reported that by using MRI it is possible to visualise magnetically labelled cells in the brain after transplantation. Rat foetal brain cells labelled with superparamagnetic iron-oxide (SPIO) were injected into intact brains (Hawrylak

et al. 1993) (Norman et al. 1992). In these studies MRI showed that the contrast agent remained primarily localised at the injection site. Oligodendrocyte progenitor cells labelled with MION-461-OX-26 and injected into the spinal cord after lesioning were shown to migrate in the spinal cord (Bulte et al. 1999b) (Bulte et al. 1998). Endorem®, which was used in the present studies, is clinically approved as a blood pool agent and does not require any facilitation of iron uptake or cell modification. The stem cells used for transplantation, MSCs and eGFP ESCs, fully retain their ability to divide in culture when labelled with Endorem®. Regardless of the administration route, nanoparticle-labelled cells were found to migrate to the lesion site, and the cells were detected by MRI. Thus, Endorem® can be used as a stem cell marker, and through non-invasive *in vivo* tracking using MRI, the fate of labelled cells can be studied following transplantation.

Electron microscopy

There are many ways to characterise cells. Using LM, their phenotypes can be examined with the help of histochemical staining and cell-specific markers. By using molecular biological techniques and *in situ* hybridisation, it is possible to quantify RNA expressions or to define DNA sequences. To solely rely on cell phenotype expression in affected tissue is risky, as in that case the assumption would be that the phenotype of an affected cell is exactly the same as that of a healthy cell. This is not necessarily true (Orenstein 2000). Furthermore, TUNEL staining used for detecting apoptosis can be transiently positive for cells undergoing necrosis, and BrdU staining for detecting dividing cells can stain damaged cells. To study the structural appearance of a cell is as important as to study the cell's phenotype, which usually is visualised only as a spot of a certain colour in optical microscopes or as a dark strip in a gel, without any distinct correlation to cell morphology. Using electron microscopes, subtle morphological changes can be studied, and employed in parallel with other research techniques, EM is a useful tool.

However, EM is a time consuming and expensive technique. The samples have to be carefully prepared through many steps to give proper details. The final ultrathin sections have to be viewed in a vacuum, as air would scatter the electrons, and therefore tissues cannot be studied *in vivo*. Due to the small sample size and the high magnification, EM images represent very selective events in time and location (Lloreta-Trull 2000) and sampling is therefore crucial.

For unbiased sample selection of the tissue, in the present studies standardised sampling procedures were developed. Since the sample orientation was randomised, the final ultrathin sections were considered to be representative of the lesion. Usually many sections have to be examined to get a true picture of the cell ultrastructure, and in many cases EM is used as a technique to confirm results obtained by other methods. Conventional histology, MRI and EM were used in parallel to examine the tissues in the present studies. MRI can reveal dynamic changes in the tissue water balance *in vivo* that are not detected by histology or EM. Also, for *in vivo* tracking of the fate of superparamagnetic nanoparticle-labelled cells, MRI is a useful technique. However, EM shows subtle morphological changes and cellular dynamics that cannot be detected by any other method. In particular, EM is a suitable tool when studying iron-oxide nanoparticle-labelled cells, since no further labelling is needed to visualise the particles at the ultrastructural level, as iron-oxide itself is a heavy metal, thus providing contrast in EM images.

CONCLUDING REMARKS

The lesion models used in the present studies are useful models for studying injured cells. Using electron microscopy, subtle morphological changes can be studied and the criteria of different cell death pathways detected. At 3 h following a cortical photochemical lesion, complete cell death was found in the core of infarction and also the ultrastructural criteria of irreversible cell death contralateral to the lesion site. At 3 h following a cortical compression lesion, secondary delayed cell death was found contralateral to the *penumbra* zone. Therefore, we suggest 3 h after lesioning to be a time breakpoint, at which cells either progress towards lethal changes or recover. Thereafter, neuronal reorganisation could be possible since metabolically active cells are still present in both hemispheres. Since the cell death, characterised as apoptosis, was delayed in time, the cells in the *penumbra* zone are also targets for therapy during the first hours after lesioning.

Historically, when investigating apoptosis, the major focus has been to examine classical apoptosis or programmed cell death during development. With the recognition that pathological cell death may share cellular features with

programmed cell death during development, there are further possibilities for therapeutic intervention. Therefore, a growing_understanding of the structural and biochemical components of the cell death pathway following CNS injury may reveal new potential strategies for the treatment of neurodegenerative disorders and neuronal loss after CNS trauma. Such therapies could include anti-apoptotic treatment by caspase inhibition using different pharmacological agents or neuroprotection by viral vectors for expressing neurotrophic factors.

The use of stem cells to replace lost neurones following injury is a promising therapeutic strategy. The present studies demonstrate that fluoxetine enhances neurogenesis and stem cell migration towards an ischemic lesion. Also, following implantation, embryonic stem cells and bone marrow stromal cells labelled with iron-oxide nanoparticles migrated to an injured site. Labelled with Endorem®, the stem cells stayed viable and MRI tracked their migration. However, when grafting stem cells, it is essential to study not only the signs of development, differentiation and migration, but also the functional repair of CNS damage. Studies of functional repair still remain limited. The first reports of the functional effects of the implantation of stem cells have been in rodent models of ischemia, in which rats showed dramatic improvements in spatial learning following stem cell transplantation. The present work showed that beam-walking training enhanced neurogenesis following ischemia and that fluoxetine and beam-walking enhanced functional recovery. However, further studies of functional repair after stem cell transplantation following lesioning and during neurogenesis have to be performed.

ACKNOWLEDGEMENTS

The work underlying this thesis was carried out at MR-Centre, Dept. of Clinical Neuroscience, Karolinska Institutet, Stockholm, Sweden and also at the Inst. of Experimental Medicine, AS CR, EU Centre of Excellence, Prague, Czech Republic. I wish to express my sincere gratitude to all that in one way or another have contributed to this work, and especially to:

Börje Bjelke, my former supervisor, MR-Centre, for encouraging me in my early studies and for introducing me into the MR field. I also would like to thank you for introducing me to Eva Syková. It turned out to be important for me;

Eva Syková, my main supervisor, Professor and Director at the Inst. of Experimental Medicine, Academy of Sciences of the Czech Republic, for being a great supportive mentor and friend. I wish to thank you for teaching me in science, for clearing up my first messy manuscript, for giving me hard times when preparing presentations, and not least, for providing me access to a frontline electron microscope. Probably, I never would have achieved this without you. I thank you also for all the nice trips and concerts we had. I never regret my travelling to Prague;

Mikael Svensson, my second supervisor, Dept. of Clinical Neuroscience, for supporting me and thus, taking "institutional responsibility". You maid it possible for me to continue my studies at the Karolinska Institutet and you firmly kept everything under control;

Martin Ingvar, Head of MR-Centre, for advising and supporting me during a troublesome period;

My friends, colleagues and co-authors at the MR-Centre (Stockholm):
Zhengguang Chen, Masahiro Abo, Li-Ju Lai, Xingchen Wu and Tomas Klason for the time we spent in the lab with experiments and MR recordings. The MR physicist: Tomas Jonsson, Stefan Skare, Magnus Karlsson, Andreas Piringer, Peter Fransson, Jesper Andersson and Gunther Helms for making MR physics understandable. I also remember our nice lunches. Stuff at the Clinical MR-centre, especially: Birgitta Löwegren, Åsa Avango, Lars Blomberg, Yords Österman and Dan Greitz for letting me be one among you;

My friends, colleagues and co-authors at the Inst of Exp. Medicine:
Pavla Jendelová, Lucia Urdzíková, Aleš Hejcl, Kate□ina Glogarová, Miroslava And□rová, Alexandr Chvátal, Zuzana Šimonová, Lýdia Varková, Katha□ina Nám□stiková, Marketa Pissnova and James Dutt. I thank you all for quickly adopting me into your lab society. It is always nice discussing with you and one day, perhaps, I will understand some Czech language. In particular I would like to thank my roommates, Lucia and Aleš, for making life easy and joyful in the lab. Marketa, I am grateful to you for your help with accommodation, visa documents and other matters. I wish to specially thank you, James, for the patience you show when reviewing my English texts, for interesting discussions and for nice dinners with your family;

My friends, colleagues and co-authors at the MR-Unit (Prague):
Milan Hájek, Filip Jiru, Vít Herynek Daniel Jirák and Martin Burian for making me feel welcome at the MR-Unit. Daniel, I thank you for showing interest in electron microscopy.

My warmest gratitude includes:

My dear friends: Birgitta Vagnhammar-Carlsson, Solveig Lind-Medina, Maria Ahlsén, Catharina Bonnemann. I thank you all for giving distraction from work and for listening to my endless stories.

My dear family: I thank you, Carlåke, for your generous support and tolerance. Certainly, I never would have achieved this without you. I thank you, Niklas, Mikael and Sofia, for being strong during the years of my studies.

We thank Stiftelsen för Strategisk Forskning, Knut och Alice Wallenbergs Stiftelse, Konung Gustav V:s och Drottning Victorias Stiftels, Grant Agency of the Czech Republic, Academy of Sciences of the Czech Republic, Ministry of Education, Sports and Youth of the Czech Republic.

REFERENCES

Abo M, Chen Z, Lai LJ, Reese T, Bjelke B. 2001. Functional recovery after brain lesion--contralateral neuromodulation: a fMRI study. Neuroreport 25;12(7):1543-1547.

Alberts B. 1989. Molecular biology of the cell. New York: Garland.

Alvarez-Buylla A, Seri B, Doetsch F. 2002. Identification of neural stem cells in the adult vertebrate brain. Brain Research Bulletin 57(6):751-758.

Auer RN, Kalimo H, Olsson Y, Siesjo BK. 1985a. The temporal evolution of hypoglycemic brain damage. I. Light- and electron-microscopic findings in the rat cerebral cortex. Acta Neuropathol (Berl) 67(1-2):13-24.

Auer RN, Kalimo H, Olsson Y, Siesjo BK. 1985b. The temporal evolution of hypoglycemic brain damage. II. Light- and electron-microscopic findings in the hippocampal gyrus and subiculum of the rat. Acta Neuropathol (Berl) 67(1-2):25-36.

Becker D, Sadowsky CL, McDonald JW. 2003. Restoring function after spinal cord injury. The Neurologist 9:1-15.

Bernhardt J, Dewey H, Thrift A, Donnan G. 2004. Inactive and alone: physical activity within the first 14 days of acute stroke unit care. Stroke Apr;35(4):1005-1009.

Björklund A, Dunnett SB, Brundin P, Stoessl AJ, Freed CR, Breeze RE, Levivier M, Peschanski M, Studer L, Barker R. 2003. Neural transplantation for the treatment of Parkinson's disease. Lancet Neurol 2(7):437-445.

Björklund A, Lindvall O. 2000. Cell replacement therapies for central nervous system disorders. Nature of Neuroscience 3:537-544.

Björklund LM, Sanchez-Pernaute R, Chung S, Andersson T, Chen IY, McNaught KS, Brownell AL, Jenkins BG, Wahlestedt C, Kim KS, Isacson O. 2002. Embryonic stem cells develop into functional dopaminergic neurons after transplantation in a Parkinson rat model. Proc Natl Acad Sci USA 99(4):2344-2349.

Bonfoco E, Krainc D, Ankarcrona M, Nicotera P, Lipton SA. 1995. Apoptosis and necrosis: two distinct events induced, respectively, by mild and intense insults with N-methyl-D-aspartate or nitric oxide/superoxide in cortical cell cultures. Proceedings of the National Academy of Sciences of the United States of America 92(16):7162-7166.

Bonnemain B. 1996. In: V.L.C., editor. Superparamagnetic and blood pool agents. Spotlight on clinical MRI. France: Maffliers. 75-82 p.

Boyeson MG, Feeney DM, Dail WG. 1991. Cortical microstimulation thresholds adjacent to sensorimotor cortex injury. J of Neurotrauma 8(3):205-217.

Brock JH. 1989. The biology of iron. Iron in immunity. Cancer and inflammation. de Sousa M, Brock JH, editors. London: Wiley. 35-53 p.

Brown AW. 1977. Structural abnormalities in neurones. J Clin Pathol 30(suppl. 11):155-169.

Brown AW, Brierly JB. 1972. Anoxic-ischemic cell change in rat brain: light microscopic and fine-structural observations. J Neurol Sci 16(1):59-84.

Brustle O, Jones KN, Learish RD, Karrman K, Choudhary K, Wiestler OD, Duncan ID, McKay RD. 1999. Embryonic stem cell-derived glial precursors: a source of myelinating transplants. Science 285(5428):754-756.

Bulte JW, Brocks RA, Moskowitz BM, Bryant LHJ, Frank JA. 1998. T1 and T2 relaxometry of monocrystalline iron oxide nanoparticles (MION-46L): theory and experiment. Acad Radiol 5:137-140.

Bulte JW, Brocks RA, Moskowitz BM, Bryant LHJ, Frank JA. 1999a. Relaxometry and magnetometry of the MR contrast agent MION-46L. Magn Reson Med 42:379-384.

Bulte JW, Bryant LH. 2001. Molecular and cellular magnetic resonance contrast agents. De Cuyper M, Bulte, J.W., editor: Kluwer academic publishers. 197-211 p.

Bulte JW, Douglas T, Wirtwer B, Zhang SC, Strable E, Lewis BK, Zywicke H, Miller B, van Gelderen P, Moskowitz BM, Duncan ID, Frank JA. 2001. Magnetodendrimers allow endosomal magnetic labeling and in vivo tracking of stem cells. Nat Biotechnol 19:1141-1147.

Bulte JW, Zhang SC, van Gelderen P, Herynek V, Jordan EK, Duncan ID, Frank JA. 1999b. Neuroptransplantation of magnetically labeled oligodendrocyte progenitors: magnetic resonance tracking of cell migration and myelination. Proc Natl Acad Sci USA 96:15256-15261.

Campenot RB, MacInnis BL. 2004. Retrograde transport of neurotrophins: fact and function. J Neurobiol Feb 5;58(2):217-229.

Carmichael TS. 2003. Plasticity of cortical projections after stroke. Neuroscientist 9(1):64-75.

Chen X, Katakowski M, Li Y, Lu D, Wang L, Zhang SC, Chen J, Xu Y, Gautam S, Mahmood A, Chopp M. 2002. Human bone marrow stromal cells cultures conditioned by traumatic brain tissue extracts: Growth factor production. J Neurosci Res 69:687-691.

Chen Z. 2001. Expermental and clinical perspective on stroke: Evaluation by behavior, magnetic resonance imaging and morphology. MR Centre. Dept. of Clinical neurosciense, Karolinska Institutet, Stockholm: Repro Print AB

Chesler M. 1990. The regulation and modulation of pH in the nervous system. Progr Neurobiol 34(5):401 - 427.

Choi DW. 1992. Excitotoxic cell death. Journal of Neurobiology 23:1261-1276.

Choi DW. 1996. Ischemia-induced neuronal apoptosis. [Review] [55 refs]. Current Opinion in Neurobiology 6(5):667-672.

Collins RC. 1989. Selective vulnerability of the brain: new insights into the pathophysiology of stroke. Ann Intern Med 110:992-1000.

Cragg BG. 1976. Ultrastructural features of human cerebral cortex. J Anat 121(2):331-362.

De Keyser J, Sulter G, Luiten PG. 1999. Clinical trials with neuroprotective drugs in acute ischaemic: are we doing the right thing. Trends Neurosci 22(12):535-540.

Doetchman TC, Eistetter H, Katz M, Schmidt W, Kelmer R. 1985. The in vitro development of blastocyst-derived embryonic stem cell lines: formation of visceral yolk sac, blood islands andmyocardium. J Embryol Exp Morphol 87:27-45.

Duchen MR. 2000. Mitochondria and calcium: from cell signalling to cell death. J Physiol Nov;15(529 Pt 1):57-68.

Eaves CJ, Cashman JD, Kay RJ, Dougherty GJ, Otsuka T, Gaboury LA, Hogge DE, Lansdorp PM, Eaves AC, Humphries RK. 1991. Mechanisms that regulate the cell cycle status of very primitive hematopoietic cells in long-term human marrow cultures. II. Analysis of positive and negative regulators produced by stromal cells within the adherent layer. Blood 78:110-117.

Fawcett J, Rosser A, Dunnett S. 2001. Brain damage, brain repair. New York: Oxford University Press Inc.

Feeney DM, Boyeson MG, Linn RT, Murray HM, Dail WG. 1981. Responses to cortical injury: I. Methodology and local effects of contusions in the rat. Brain Res 27;211(1):67-77.

Frank JA, Miller BR, Arbab AS, Zywicke HA, Jordan EK, Lewis BK, Bryant LH, Bulte JW. 2003. Clinically applicable labeling of mammalian and stem cells by combining superparamagnetic iron oxide and transfection agents. Aug;228(2):480-487.

Frisen J, Johansson CB, Lothian C, Lendahl U. 1998. Central nervous system stem cells in the embryo and adult. Cell Mol Life Sci Sep;54(9):935-945.

Fuxe K, Agnati LF. 1991. Volume transmission in the brain: novel mechanisms for neuronal transmission. New York: Raven Press, Ltd.

Gage FH. 2000. Mammalian neural stem cells. Science Feb 25;287(5457):1433-1438.

Gage FH. 2002. Neurogenesis in adult brain. J Neuroscience 22(3):612-613.
Garcia JH, Liu KF, Ho KL. 1995. Neuronal necrosis after middle cerebral artery occlusion in Wistar rats progresses at different time intervals in the caudoputamen and the cortex. Stroke 26(4):636-643.
Garcia JH, Lossinsky AS, Kauffman FC, Conger KA. 1978. Neuronal ischemic injury: light microscopy, ultrastructure and biochemistry. Acta Neuropathol (Berl) 7;43(1-2):85-95.
Garcia JH, Yoshida Y, Chen H, Li Y, Zhang ZG, Lian J, Chen S, Chopp M. 1993. Progression from ischemic injury to infarct following middle cerebral artery occlusion in the rat. Am J Pathol 142(2):623-635.
Ghadially FN. 1975. Ultrastructural Pathology of the Cell. London: Butterworth & Co Ltd.
Ginsberg MD. 1990. Local metabolic responses to cerebral ischemia. Cerebrovasc Brain Metab Rev 2(1):58-93.
Ginsberg MD, Pulsinelli WA. 1994. The ischemic penumbra, injury thresholds, and the therapeutic window for acute stroke. Ann Neurol 36(4):553-554.
Gould E, Gross CG. 2002. Neurogenesis in adult mammals: some progress and problems. The Journal of Neuroscience 22(3):619-623.
Hakim AM. 1998. Ischemic penumbra: the therapeutic window. Neurology 51(3 Suppl 3):S44-46.
Hawrylak N, Ghosh P, Broadus J, Schlueter C, Greenough WT, Lauterbur PC. 1993. Nuclear magnetic resonance (NMR) imaging of iron oxide-labeled neural transplants. Exp Neurology 121:81-92.
Himi T, Ishizaki Y, Murota SI. 1998. A caspase inhibitor blocks ischemia-induced delayed neuronal death in gerbils. European Journal of Neuroscience 10:777-781.
Hofstetter CP, Schwarz EJ, Hess D, Widenfalk J, El Manira A, Prockop JD, Olson L. 2002. Marrow stromal cellsform guiding strands in the injured spinal cord and promote recovery. Proc Natl Acad Sci USA 96:2199-2204.
Isacson O. 2003. The production and use of cells as therapeutic agents in neurodegenerative diseases. Lancet Neurol 2(7):417-424.
Johansson CB. 2003. Mechanism of stem cells in the central nervous system. J Cell Physiol Sep;196(3):409-418.
Judd MG, Nagaraja TN, Brookes N. 1996. Potassium-induced stimulation of glutamate uptake in mouse cerebral astrocytes: the role of intracellular pH. J Neurochem Jan;66(1):169-176.
Kalimo H, Garcia JH, Kamijyo Y, Tanaka J, Trump BF. 1977. The ultrastructure of "Brain Death". II. Electron microscopy of feline cortex after complete ischemia. Virchovs Arch B Cell Pathol 3;25(3):207-220.
Kermer P, Klocker N, Bahr M. 1999. Neuronal death after brain injury. Models, mechanisms, and therapeutic strategies in vivo. Cell Tissue Res 298(3):383-395.
Kerr JF, Wyllie AH, Currie AR. 1972. Apoptosis: a basic biological phenomenon with wide-ranging implications in tissue kinetics. Br J Cancer 26(4):239-257.
Kirino T, Sano K. 1984. Fine structural nature of delayed neuronal death following ischemia in the gerbil hippocampus. Acta Neuropathol (Berl) 62(3):209-218.
Kraig RP, Chesler M. 1990. Astrocytic acidosis in hyperglycemic and complete ischemia. J Cereb Blood Flow Metab 10(1):104-114.
Kundrotiené J, Wägner A, Liljequist S. 2002. Extradural compression of sensorimotor cortex: A useful model for studies on Ischemic brain damage and neuroprotection. J Neurotrauma 19(1):69-84.
Kuroda S, Siesjo BK. 1997. Reperfusion damage following focal ischemia: pathophysiology and therapeutic windows. Clin Neurosci 4(4):199-212.

Lee JM, Zipfel GJ, Choi DW. 1999. The changing landscape of ischaemic brain injury mechanisms. Nature 24;399(6738 Suppl):A7-14.
Leitch AR. 2000. Higher levels of organization in the interphase nucleus of cycling and differentiated cells. Microbiology and molecular biology reviews March:138-152.
Li Y, Chopp M, Wang L, Gautam SC, Xu YX, Zhang Z. 2000. Intrastriatal transplantation of bone marrow nonhematopoietic cells improves functional recovery after stoke in adult mice. J Cereb Blood Flow Metab 20:1311-1319.
Lipton P. 1999. Ischemic cell death in brain neurons. Physiol Rev 79(4):1431-1568.
Lloreta-Trull J. 2000. Electron microscopy in pathology articles: a retrospective appraisal. Ultrastrct Pathol 24:105-108.
Lu D, Mahmood A, Wang L, Li Y, Lu M, Chopp M. 2001. Adult bone marrow stromal cells administrated intravenously to rats after traumatic brain injury migrate into brain and improve neurological outcome. Neuroreport 12:559-563.
MacManus JP, Linnik MD. 1997. Gene expression indused by cerebral ischemia: an apoptotic perspective. J Cereb Blood Flow Metab 17:815-832.
Malberg JE, Eisch AJ, Nestler EJ, Duman RS. 2000. Chronic antidepressant treatment increases neurogenesis in adult rat hippocampus. The Journal of Neuroscience 20(24):9104-9110.
Marzella L, Glaumann H. 1981. Effects of in vivo liver ischemia in microsomes and lysosomes. Virchows Arch Cell Pathol 36:1-25.
Maysinger D, Berezovskaya O, Fedoroff S. 1996. The hematopoietic cytokine colony stimulating factor 1 is also a growth factor in CNS: (II). Microen capsulated CSF-1 and LM-10 cells as delivery systems. Exp Neurology 141:47-56.
Mazel T, Richter F, Vargova L, Syková E. 2002. Changes in extracellular space volume and geometry induced by cortical spreading depression in immature and adult rats. Physiol Res 51(suppl 1):85-93.
McDonald JW, Liu XZ, Qu Y, Liu S, Mickey SK, Turetsky D, Gottlieb DI, Choi DW. 1999. Transplanted embryonic stem cells survive, differentiate and promote recoveryin injured rat spinal cord. Nat Med 5(12):1410-1412.
Moseley ME, Kucharczyk J, Mintorovitch J, Cohen Y, Kurhanewicz J, Derugin N. 1990. Diffusion-weighted MR imaging of acute stroke; correlation with T2-wighted and magnetic susceptibility-enhanced MR imaging in cats. American Journal of Neuroradiology 11:423-429.
Nakatomi H, Kuriu T, Okabe S, Yamamoto S, Hatano O, Kawahara N, Tamura A, Kirino T, Nakafuku M. 2002. Regeneration of hippocampal pyramidal neurons after Ischemic brain injury by recruitment of endogenous neural progenitors. Cell 110:429-441.
Newcomb JK, Zhao X, Pike BR, Hayes RL. 1999. Temporal profile of apoptotic-like changes in neurons and astrocytes following controlled cortical impact injury in the rat. Exp Neurol 158(1):76-88.
Nhan H, Barquist K, Bell K, Esselman P, Odderson IR, Cramer SC. 2004. Brain function early after stroke in relation to subsequent recovery. J Cereb Blood Flow Metab Jul;24(7):756-763.
Nicholson C, Syková E. 1998. Extracellular space revealed by diffusion analysis. Trends Neurosci 21(5):207-215.
Nitatori T, Sato N, Waguri S, Karasawa Y, Araki H, Shibanai K, E. k, Uchiyama Y. 1995. Delayed neuronal death in the CA1 pyramidal cell layer of the hippocampus following transient ischemia is apoptosis. J Neurosci 15(2):1001-1011.
Norman AB, Thomas SR, Pratt RG, Lu SY, Norgren RB. 1992. Magnetic resonance imaging of neural transplants in rat brain using superparamagnetic contrast agent. Brain Res 594:279-283.

Orenstein JM. 2000. Isn't a picture still worth a thousand words. Ultrastructural Pathology 24:67-74.
Paxinos G, Watson C. 1986. The rat brain in stereotaxic coordinates. Sydney: Academic Press.
Pencea V, Bingaman KM, Freedman LJ, Luskin MB. 2001. Neurogenesis in the subventricular zone and rostral migrator stream of the neonatal and adult primate forebrain. Exp Neurol 172(1):1-16.
Petito CK, Pulsinelli WA. 1984. Sequential development of reversible and irreversible neuronal damage following cerebral ischemia. J Neuropathol Exp Neorol 43(2):141-153.
Pleasure JS, Anderson S, Hevner R, Bagri A, Marin O, Lowenstein DH, Rubenstein JLR. 2000. Cell migration from ganglionic eminences is required for development of hippocampal GABAergic interneurons. Neuron 28:727-740.
Provenzale JM, Sorensen AG. 1999. Diffusion-weighted MR imaging in acute storke: theoretic considerations and clinical applications. AJR Am J Roentgenol 173(6):1459-1467.
Rietze R, Poulin P, Weiss S. 2000. Mitotically active cells that generate neurons and astrocytes are present in multiple regions of the adult mouse hippocampus. J Comp Neurol 28;424(3):397-408.
Rothman SM, Olney JW. 1987. Excitotoxicity and the NMDA receptor. Trends Neurosci 10:299-302.
Silani V, Leigh N. 2003. Stem cell therapy for ALS: hope and reality. Amyotroph Lateral Scler Other Motor Neuron Disord 4(1):8-10.
Studzinski GP. 1999. Apoptosis, a practical approach. Hames BD, editor. New York: Oxford University Press Inc.
Sugawara T, Chan PH. 2003. Reactive oxygen radicals and pathogenesis of neuronal death in cerebral ischemia. Antioxid Redox Signal Oct;5(5):597-607.
Syková E. 1997. The extracellular space in the CNS: its regulation, volume and geometry in normal and pathological neuronal function. The Neuroscientist 3(1):28-41.
Syková E. 2004. Diffusion properties of the brain in health and disease. Neurochem Int Sep 45(4):453-466.
Syková E, Chvatal A. 2000. Glial cells and volume transmission in the CNS. Neurochem Int Apr;36(4-5):397-409.
Taira Y, Marsala M. 1996. Effect of proximal arterial perfusion pressure on function, spinal cord blood flow, and histopathological changes after increasing intervals of aortic occlusion in the rat. Stroke 27:1850-1858.
Taupin P, Gage FH. 2002. Adult neurogenesis and neural stem cells of the central nerous system in mammals. J Neurosci Res 69(6):745-749.
Temple S. 2001. The development of neural stem cells. Nature 1;414(6859):112-117.
van Bruggen N, Cullen BM, King MD, Doran M, Williams SR, Gadian DG, Cremer JE. 1992. T2- and diffusion-weighted magnetic resonance imaging of a focal ischemic lesion in rat brain. Stroke 23(4):576-582.
van der Toorn A, Syková E, Dijkhuizen RM, Vorisek I, Vargova L, Skobisova E, van Lookeren Campagne M, Reese T, Nicolay K. 1996. Dynamic changes in water ADC, energy metabolism, extracellular space volume, and tortuosity in neonatal rat brain during global ischemia. Magn Reson Med Jul;36(1):52-60.
van Praag H, Kempermann G, Gage FH. 1999. Running increases cell proliferation and neurogenesis in the adult mouse dentate gyrus. Nature Neurosciense 2:266-270.
van Praag H, Schinder AF, Christie BR, Toni N, Palmer TD, Gage FH. 2002. Functional neurogenesis in adult hippocampus. Nature 415(6875):1030-1034.

Vanicky I, Urdzikova L, Saganova K, Cizkova D, Galik J. 2001. A simple and reproducible model of spinal cord injury induced by epidural balloon inflation in the rat. J Neurotrauma 18(12):1399-1407.

Vorisek I, Hajek M, Tintera J, Nicolay K, Syková E. 2002. Water ADC, extracellular space volume, and turtuosity in the rat cortex after traumatic injury. Magn Reson Med 48(6):994-1003.

Wang YX, Hussain SM, Krestin GP. 2001. Superparamagnetic iron oxide contrast agents: physiocochemical characteristics and applications in MR imaging. Eur Radiol 11(11):2319-2331.

Watson BD, Dietrich WD, Busto R, Wachtel MS, Ginsberg MD. 1985. Induction of reproducible brain infarction by photochemically initiated thrombosis. Ann Neurol 17(5):497-504.

Weissleder R, Cheng HC, Bogdanova A. 1997. Magnetically labeled cells can be detected by MR imaging. J Magn Reson Imaging 7(1):258-263.

Yang SY, Xue L. 2004. Human neuronal apoptosis secondary to traumatic brain injury and the regulative role of apoptosis-related genes. Chin J Traumatol Jun;7(3):159-164.

Yeh T, Zhang W, Ildstad ST, Ho C. 1993. Intracellular labeling of T-cells with superparamagnetic contrast agents. Magn Reson Med 30:617-625.

Yeh T, Zhang W, Ildstad ST, Ho C. 1995. In vivo dynamic MRI tracking of rat T-cells labeled with superparamagnetic iron-oxide particles. Magn Reson Med 33:200-208.